Adhesion and stiction: Mechanisms, measurement techniques, and methods for reduction

Bharat Bhushan[a)]
Nanotribology Laboratory for Information Storage and MEMS/NEMS, The Ohio State University, 206 W 18th Avenue, Columbus, Ohio 43210-1107

(Received 8 May 2003; accepted 29 September 2003; published 24 November 2003)

Solid±solid adhesion occurs at contacting asperities in two contacting solids. A thin liquid ®lm with a small contact angle, present at the interface, can result in the so-called liquid-mediated adhesion. This may result in high adhesion during normal pull and high static friction during sliding, both commonly referred to as ``stiction." The problem of high stiction is especially important in an interface involving two very smooth surfaces under lightly loaded conditions. This article provides a critical and comprehensive review of mechanisms of adhesion and stiction, various measurement techniques, and methods used to reduce stiction in magnetic storage devices and micro/nanoelectromechanical systems. • *2003 American Vacuum Society.* [DOI: 10.1116/1.1627336]

I. INTRODUCTION

When two nominally ¯at surfaces with asperities and valleys are placed in contact, surface roughness causes contacts to occur at discrete contact spots. The sum of the areas of all the contact spots constitutes the real (true) area of contact or simply contact area, A_r, which is a small fraction of apparent area A_a. The load is supported by the deformation at the tips of the contacting asperities (Fig. 1). The proximity of the asperities results in adhesive contacts caused by interatomic attractions. In a broad sense, adhesion is considered to be either physical or chemical in nature. Experimental data suggest that adhesion is primarily due to weak van der Waals forces.[1±4] Because of adhesion or bonding across the interface a ®nite normal force is required to pull the two solids apart.

If there is a liquid present and it wets the surface ($0 \leqslant \theta < 90$É, where θ is the contact angle between the liquid and surface), the surface is referred to as hydrophilic (water loving), and if it does not wet ($\theta \geqslant 90$É), the surface is referred to as hydrophobic (water fearing). With the presence of a thin liquid ®lm between two ¯at surfaces, curved menisci form around contacting and noncontacting asperities due to surface energy effects; see Fig. 2. The meniscus is concave shaped for an interface with hydrophilic surfaces and is convex for hydrophobic surfaces. For an interface with hydrophilic surfaces, the attractive meniscus force arises from the negative Laplace pressure inside the curved (concave) meniscus as a result of surface tension. The product of this pressure difference and the immersed surface area is the attractive (adhesive) force as a result of liquid mediated adhesion, and is referred to as the meniscus force.[5,6] In some cases, this attractive force may be large as compared to that of solid±solid contact.[2]

When two contacting surfaces move relative to each other, frictional force, commonly referred to as ``intrinsic" or ``conventional" frictional force, is contributed by adhesion and deformation of the contacting asperities [Fig. 3(a)]. For most practical cases, the adhesional component of friction is the primary contributor.[2±4] Figure 3(b) also shows tangential force versus time or displacement. In some cases, the static friction force required to initiate sliding is larger than the kinetic friction force required to sustain sliding. In addition, in the presence of a thin liquid ®lm, high static friction can occur due to meniscus/viscous effects; this is referred to as ``stiction." [1±4,7,8] The problem of high adhesion during normal pull and high static friction (stiction) during sliding in liquid-mediated contacts is particularly important in an interface involving two very smooth surfaces under lightly loaded conditions. The word ``stiction" was coined at IBM General Products Division labs in San Jose, CA around 1980 when they encountered that head slider getting stuck to the disk surface while resting at high humidities due to liquid mediated adhesion.[2] High lateral force had to be applied to initiate sliding to overcome high static friction or sticking, hence leading to the term stiction.

Mechanisms of solid±solid adhesion have been studied over the last half a century and a good understanding exists.[9±15] Because of the use of smooth surfaces and lightly loaded conditions, liquid-mediated adhesion and stiction presented concern in the magnetic storage industry in the early 1980s,[2] and is gaining importance in the emerging micro/nanoelectromechanical systems (MEMS/NEMS) industry.[16±23] In micro/nanoscale drug delivery devices (BioMEMS/NEMS) under development, adhesion between these devices and disease cells, referred to as bioadhesion, is required. Bioadhesion is de®ned as the adherence of molecules to biological surfaces. Few papers on these devices and bioadhesion issues exist.[19,24±26]

The objective of this paper is to provide a critical and comprehensive review of the mechanisms of adhesion and stiction, various stiction measurement techniques, and methods used to reduce stiction in magnetic storage devices and the MEMS/NEMS industry.

a)Electronic mail: bhushan.2@osu.edu

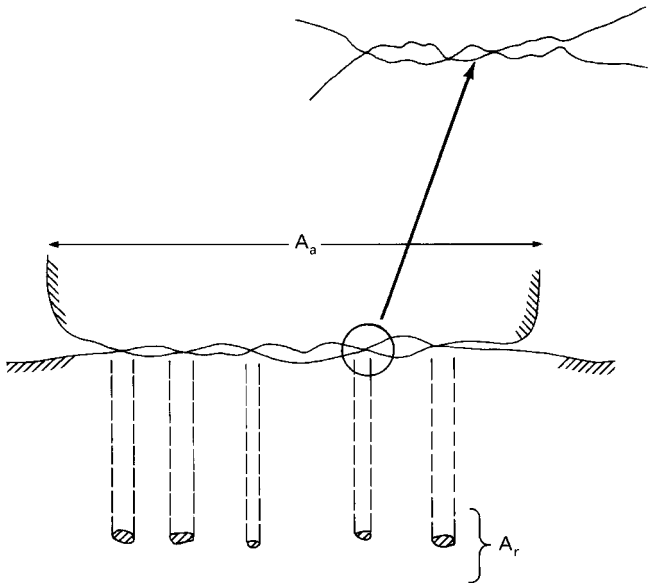

FIG. 1. Schematic of two rough surfaces in contact and corresponding contact areas.

II. MECHANISMS OF SOLID±SOLID AND LIQUID-MEDIATED ADHESION

When two solid surfaces are brought into contact, adhesion or bonding across the interface can occur. A ®nite normal force is required to overcome adhesion, in order to pull the two solids apart; see Fig. 4.[3,4] The ratio of the normal tensile force W' required for separation (normally referred to as adhesive force) to the normal compressive force W initially applied is often referred to as the coef®cient of adhesion, μ',

$$\mu' = \frac{W'}{W}. \tag{1}$$

W′ typically increases linearly with an increase of W and μ' generally increases with duration of static contact and separation rate.

Adhesion occurs both in solid±solid contacts and in contacts involving two solids interposed with liquids or tacky solids. If two solid surfaces are clean and all of the chemical ®lms and adsorbates are removed, strong adhesion or bonding of one solid to another generally occurs. Surface contaminants or thin ®lms in many cases reduce adhesion; however, in some cases, the opposite, may be true. With well-lubricated surfaces, weak adhesion is generally observed.

Adhesion can be either desirable or undesirable. Strong adhesion is required to bond the two surfaces together. In many engineering applications such as sliding and rotating machinery, however, adhesion is undesirable. Adhesion results in friction and wear. In some applications, controlled adhesion is required.

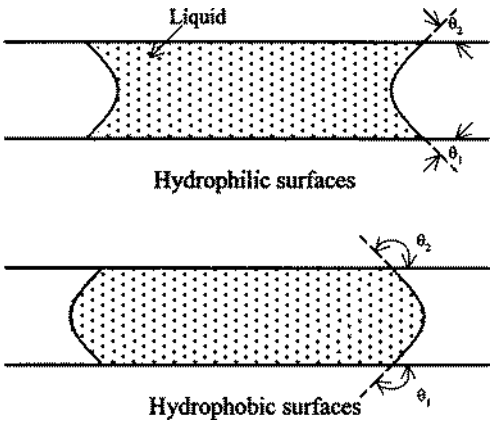

FIG. 2. Meniscus formation from a thin liquid ®lm between two ¯at surfaces.

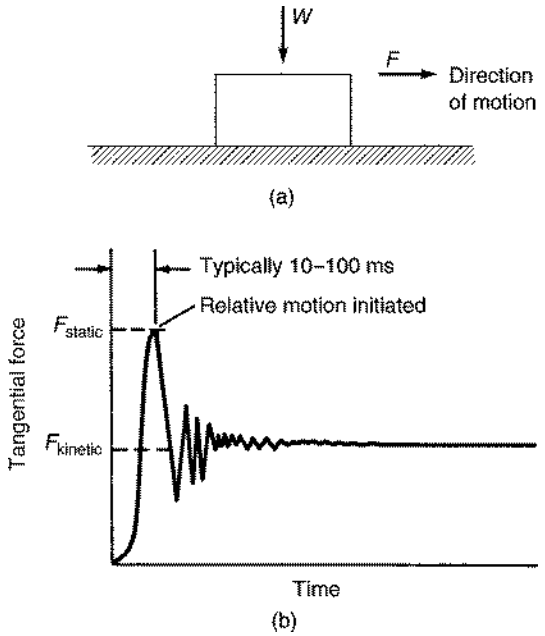

FIG. 3. (a) Schematic illustration of a body sliding on a horizontal surface, where W is the normal load (force) and F is the tangential force experienced by the body; and (b) tangential force vs time or displacement. F_{static} is the force required to initiate sliding and $F_{kinetic}$ is the force required to maintain sliding.

A. Solid±solid contact

The proximity of the asperities results in an adhesive joint caused by interatomic attractions. In a broad sense, adhesion is considered to be either physical or chemical in nature.[2±6,9,11,13,14,27±29] Chemical interaction involves cova-

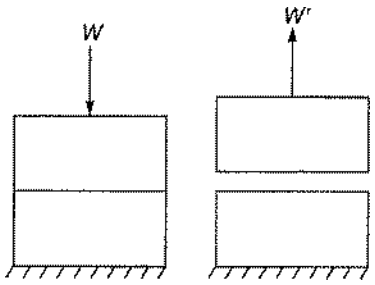

FIG. 4. Schematic illustration of normal pull of two solid bodies; W is the compressive normal force (load) applied for a certain duration and W' is the tensile normal force needed to separate surfaces.

lent bonds, ionic or electrostatic bonds, and metallic bonds. Physical interaction involves the hydrogen bonds and van der Waals bonds as a result of intermolecular forces (secondary forces of attraction). Hydrogen bonds and van der Waals bonds are much weaker than that in the molecules that undergo chemical interaction, because in these bonds there is no electron exchange. van der Waals forces are always present when two asperities are in close proximity. For two solid surfaces in contact, the interfacial bond may be stronger than the cohesive bond in the cohesively weaker of the two materials. In that case, separation of the two solids results in the transfer of the cohesively weaker material to the cohesively stronger. Adhesion is a function of material pair and interface conditions such as crystal structure, crystallographic orientation, solubility of one material into another, chemical activity and separation of charges, surface cleanliness, normal load, temperature, duration of contact (rest time or dwell time), and separation rate.[14,30]

For clean surfaces, free from oxide and other surface ®lms and from adsorbed gases, signi®cant adhesion is observed between metal surfaces; such conditions can be achieved under ultrahigh vacuum. Surface ®lms, such as physisorbed, chemisorbed and chemically reacted ®lms, and contaminants in the environment, generally decrease the adhesion of two reactive surfaces.[14,31±33] When exposed to ambient air, even noble metals adsorb oxygen and water vapor; this ®lm may not be more than a few molecules thick. Small amounts of contaminants may be much more effective in reducing the adhesion of some metals than of others. For example, a very small amount of oxygen (perhaps enough to give a monolayer) can produce a marked reduction in the adhesion of iron, whereas far more oxygen is required to produce a comparable reduction in the adhesion of copper.[3,4,14]

Temperature affects the adhesive strength of a contact. At high temperatures, softening of surfaces results in greater ¯ow, ductility, and a larger real area of contact which results in stronger adhesion. High temperatures can also result in diffusion across the interface. In a metal±metal contact, high temperature may result in increased solubility, and in a polymer±polymer contact, interdiffusion strengthens the contact, which results in stronger adhesion.

If two surfaces are placed together, because of surface roughness, the real area of contact is usually very much smaller than the geometrical area. Adhesion is affected by the real area of contact, which is a function of normal load, surface roughness, and mechanical properties.[3,4] Adhesion force generally increases linearly with an increase in the normal load; see Fig. 5(a).[34] Materials with higher roughness, modulus of elasticity and/or hardness and lack of ductility exhibit lower real area of contact, which leads to lower adhesion. Any viscoelastic or viscoplastic deformation (creep) under load would increase the real area of contact as a function of duration of contact leading to an increase in adhesion; see Fig. 5(b).[34,35] The real area of contact can also increase as a result of interatomic attraction (van der Waals or vdw forces) in the case of a soft solid, such as an elastomer, that is in contact with a hard surface, both being smooth so that

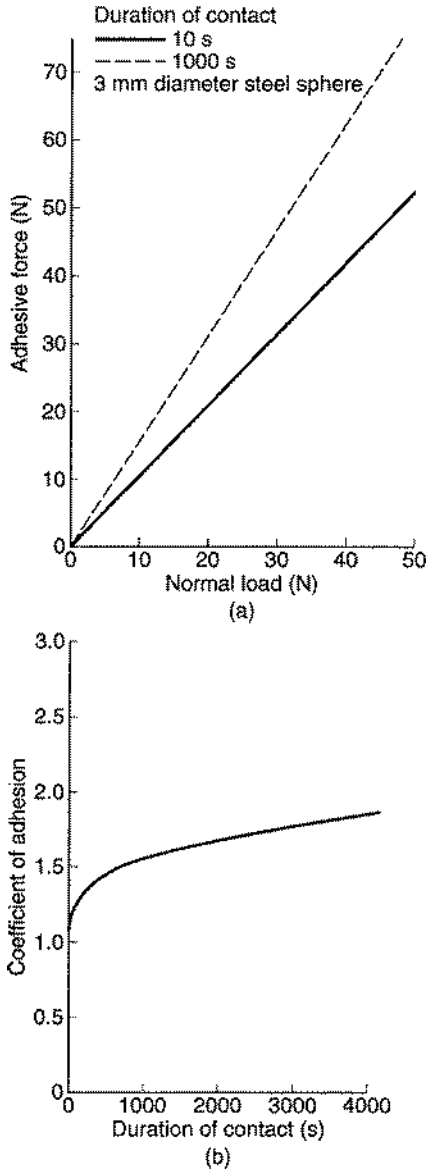

FIG. 5. (a) Adhesive force as a function of normal load, and (b) coef®cient of adhesion as a function of duration of contact for a clean steel sphere on indium (Ref. 34).

the asperity separation is on the order of molecular levels (1±10 nm)[1]. Contact ®rst occurs at the tip of the asperities. These are then drawn closer as a result of the van der Waals forces, with a normal pressure on the order of 1 atm, when asperity contacts are separated by 1±10 nm. This process goes on and may result in a very large contact area at no normal loads (Fig. 6). This mechanism is also partially responsible for the behavior of thin polymer ®lms, such as cling®lm wrap. Of course, this mechanism would be inoperative for hard material pairs and/or rough surfaces.

Another consideration in the real area of the contact is elastic recovery. When a normal force is decreased from two surfaces in intimate contact, contact is partially peeled apart by elastic forces in a process known as elastic recovery; see Fig. 7.[32] A lower elastic modulus would result in less elastic recovery and vice versa. Ductility also plays a role: the

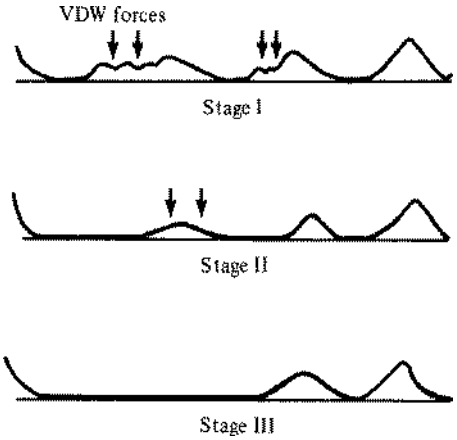

FIG. 6. Diagram indicating how the real area of contact between a smooth elastomer and a smooth hard surface grows to a larger fraction of the geometric area.

greater the ductility, the greater the elongation of the contacts and, therefore, less elastic recovery. Therefore, elasticity and ductility affect the real area over which adhesion occurs and in¯uence adhesion and friction. Elastic recovery, to a large extent, is responsible for lower adhesion of clean interfaces than the theoretical values.

Adhesive forces signi®cantly increase if a shear displacement (force) is added in addition to the normal load. When a tangential force is applied to the loaded metallic specimens, there is a growth in the real area of contact by plastic ¯ow under the in¯uence of combined normal and tangential stresses[3,4] and any relative sliding tends to produce penetration of surface layers that otherwise prevent metal-to-metal contact.[30,32] Even hard metals subjected to sliding or twisting after being pressed can exhibit high adhesion.

Now, we discuss various physical and chemical interactions that are responsible for solid±solid adhesion.

1. Covalent bond

A covalent bond consists of a pair of electrons (of opposite magnetic spins) shared between two atoms.[3,4,36,37] When covalent solids are brought into intimate contact, one might expect the bonding across the interface to be similar to the bonding within the solid. Most covalent solids have a high elastic modulus and are generally extremely hard. Consequently it is often dif®cult to obtain large areas of contact even if appreciable joining loads are employed. However, molecularly smooth surfaces can result in high real area of contact, leading to high adhesion.

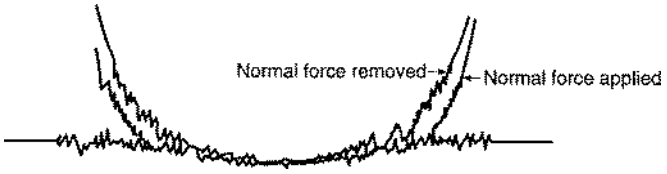

FIG. 7. Schematic showing a sphere on a nominally ¯at surface with normal force applied and the force removed.

2. Ionic or electrostatic bond

Ionic bonds are formed whenever one or more electrons are transferred from one atom to another. Transfer of electrons results in formation of negative and positive ions. Coulombic attraction of unlike ions results in the formation of ionic bonds.[3,4,36,37] Metals, which have relatively little attraction for their valence electrons, tend to form ionic bonds when they combine with nonmetals. When the separation equals the atomic spacing, the bond resembles that within the bulk of the material. If a polymer (insulator) is brought into contact with a metal, there is a far larger separation of charge at the interface. This produces an electrostatic attraction in addition to the van der Waals interaction between the bodies.[13,38±41] Based on detailed experiments with polymers, Derjaguin *et al.*[13] state that practically the whole of the adhesion is electrostatic in origin.

Transfer of charge occurs by contact and separation of two surfaces. Certain material combinations, generally nonconductive materials, become electrically charged, by friction, being rubbed. This effect is commonly referred to as the ``triboelectric effect," and is a common source of static charge generation. Being electrically charged, either negatively or positively, upon contact with an uncharged object or one of opposite polarity, there may be a discharge of static electricity, a spark. These nonequilibrium static charges will decay with time and do not result in permanent adhesion.

3. Metallic bond

The valence electrons of metals are not bound to any particular atom in the solid and are free to drift throughout the entire metal, referred to as delocalized electrons. They form a sea of electrons or an electron cloud. The remaining nonvalence electrons and atomic nuclei form ion cores which possess a net positive charge, equal in magnitude to the total valence electron charge per atom. The free electrons shield the positive ion cores from mutually repulsive electrostatic forces. The metal can be viewed as containing a periodic structure of positive ions surrounded by a sea of valence electrons (negative). The attraction between the two provides the metallic bond.[3,4,36,37]

Broadly speaking, most clean metals stick strongly to one another. For separations greater than, say, 2 nm they are attracted by van der Waals forces, which increase as the separation decreases. At a small separation the metallic bond begins to develop. When the surfaces are at an atomic distance apart, the full metallic bond is generally formed and the short-range repulsive forces also come into operation to provide ®nal equilibrium between the two bodies. If clean identical metals (e.g., gold) are pressed together with a force to produce plastic deformation at the contact region, one would expect an interfacial strength comparable with that of bulk metal, so that the force required to pull two surfaces apart should be large; it is always appreciably less, however. The effect of released elastic stresses, surface roughness, and degree of cleanliness are some of the reasons for adhesive strength being lower than expected. The ductility of the metals is important, particularly if the loading is suf®cient to

produce plastic deformation. Adhesion of ductile materials such as indium, lead, copper, and gold is generally stronger than for less ductile metals, for example, the hexagonal metals with a small number of slip systems and ceramics.

The self-adhesion of a wide range of metals seems to fall into fairly well-de®ned groups, depending on structure; for example, hexagonal metals form a self-consistent, poorly adhering group. In particular, cobalt (hcp) exhibits markedly low adhesive forces when brought in contact with itself. In general, similar metal pairs with nonhexagonal structures are metallurgically compatible and exhibit high adhesion and must be avoided, particularly iron against iron.[3,4,42]

The orientation at the surface in¯uences adhesive behavior. Like planes in contact with like planes exhibit higher adhesive bonding forces than dissimilar crystallographic planes of the same metal in contact with itself. The lowest adhesion force is found on the close-packed, high atomic density and low free surface energy planes. The polycrystalline form of a metal in contact with itself exhibits higher adhesive forces than single crystals in contact with themselves; this re¯ects the in¯uence of grain boundary energies.

In the case of dissimilar metals, the mutual solubility of metals would affect adhesion; mutually insoluble metals would generally show poor adhesion.[42±44] However, if the surfaces are thoroughly clean, regardless of mutual solubility, the adhesion would be strong. In general, but not always, transfer occurs from the softer metal to the harder metal. With some alloys, preferential segregation of one of the constituents could occur at the free surface.

4. Hydrogen bond

Hydrogen can exist both as a positively charged and as a negatively charged ion. The positive hydrogen ion, or proton, results from the removal of the only electron. The negative ion, on the other hand, is formed by the imperfect shielding of the positively charged nucleus by the single electron in the neutral atom. This imperfect shielding will result in a constantly shifting dipole that has a weak tendency to acquire another electron by purely ionic attraction. This property of the hydrogen atom enables it to bridge two negative ions in what is known as a hydrogen bond.[3,4,6,36,37] It plays an important role in adhesion with polymers if there are certain polar atoms present capable of producing hydrogen bonding. Hydrogen bonds or hydrogen bridges are the strongest secondary forces of attraction.

Hydrophilic silica surfaces in MEMS contain adsorbed water layers. When two of these hydrated surfaces are brought into close contact, hydrogen bonds may form between oxygen and the hydrogen atoms of the adsorbed water layers. Hydrogen bonds are productively used in wafer bonding.

5. van der Waals bond

The ®rst three types of bonding mentioned so far are all relatively strong primary bonds followed by hydrogen bonding. Weaker, secondary bonds, which also result in interatomic attraction, are van der Waals forces. These act between molecules or within molecules with atoms between which chemical bonds have not formed.[3,4,6,36,37] With polar molecules they arise from dipole±dipole interactions. With nonpolar molecules, they arise from the interaction of ¯uctuating dipoles in the individual atoms (London forces). For two parallel surfaces separated by a distance d, the force per unit area is

$$F_{\mathrm{vdw}}=\begin{cases} A/6\pi d^3 & \text{for } d\leqslant 30 \text{ nm} \\ B/d^4 & \text{for } d>30 \text{ nm}, \end{cases} \tag{2}$$

where A and B are the Hamaker constants. For purely van der Waals solids, A is on the order of 10^{-12} ergs, which holds true for most hydrocarbons. This equation can be used right down to atomic contact.[45]

The existence of van der Waals forces between macroscopic bodies, such as crossed mica cylinders, has been measured by several investigators.[6,46] The effect of surface roughness on van der Waals forces has been studied by Meradudin and Mazur.[47] Based on calculations, they found that surface roughness increases the magnitude of the van der Waals force over its value when the two surfaces are smooth.

6. Free surface energy theory of adhesion

A detailed calculation of van der Waals forces is dif®cult. A simpler approach is to use the concept of free surface energy.[3,4,42] If one cleaves a crystalline solid along its cleavage plane, two highly chemically active surfaces are generated. The cleavage process causes the fracture of cohesive bonds across the cleavage interface, and these fractured bonds leave the surface in a highly energetic state. Thus, the energy that normally would be associated with bonding to other atoms (like other atoms in the bulk solid) is now available at the atoms on the surface. This energy required to create a new surface, expressed over an area consisting of many atoms in the surface lattice, is referred to as free surface energy. It is a function of the material as well as the surface orientation.

Because the atoms at the surface have this unused energy, they can interact with each other, with other atoms from the bulk, and with species from the environment. Free surface energy in¯uences adhesive bonds for solids in contact and, hence, friction and wear. In addition, it determines the nature of the interaction of lubricants with solids. When a bond is formed between two materials [having free surface energies per unit area in air $(\gamma_{\mathrm{SA}})_1$ and $(\gamma_{\mathrm{SA}})_2$ or simply γ_1 and γ_2] in contact, the surface energy of the interface per unit area changes to γ_{12}. Based on early work by Bradley[48] and Bailey,[49] work of adhesion or the energy of adhesion per unit area is de®ned as

$$W_{\mathrm{ad}}=\Delta\gamma=\gamma_1+\gamma_2-\gamma_{12}, \tag{3}$$

where $\Delta\gamma$ is equal to a reduction in the surface energy of the system per unit area (always negative), in mJ/m^2, erg/cm^2, dyn/cm, or mN/m (1 mJ/m^2=1 erg/cm^2=1 dyn/cm=1 mN/m). Thus, $\Delta\gamma$ represents the energy that must be applied to separate a unit area of the interface or to create new surfaces. For two similar materials, $\Delta\gamma$ becomes the work of cohesion,

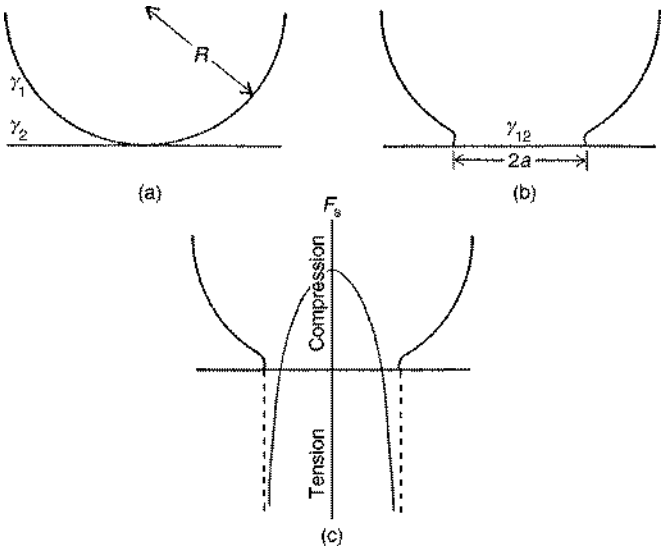

FIG. 8. Contact between elastic sphere and hard ¯at surface with no applied force: (a) in the absence of attractive forces between the two bodies, (b) in the presence of attractive forces, surfaces are drawn together to make contact over a circle of radius *a*, and (c) pressure distribution in the presence of attractive forces.

and is equal to $2\gamma(\gamma_{12}=0)$. This important thermodynamic relation [Eq. (3)] is valid for both solid and liquid interfaces. γ is generally called free surface energy for solids and surface tension for liquids. McFarlane and Tabor[34] and Sikorski[30] have reported a good correlation between the coef®cient of adhesion and W_{ad}/H_s for metal±metal pairs where H_s is the hardness of the softer metal. The exception was the hcp metals pair which exhibited low values of coef®cients of adhesion.

The higher the surface energy of a solid surface, the stronger the bonds it will form with a mating material. One obvious suggestion from the surface energy theory of adhesion is to select materials that have a low surface energy and low $\Delta\gamma$. Use of lubricants at the interface reduces the surface energy. The surface energy of solid surfaces typically ranges from a few hundred to a few thousand mJ/m^2, whereas for most liquids it is few tens of mJ/m^2. Nonpolar lubricants have a lower surface energy than polar lubricants. Organic contaminants can also reduce the surface energy considerably.

Contact analysis. We consider two elastic spheres in contact under zero external load, as shown in Fig. 8(a). Because of a decrease in the surface energy during contact, an attractive molecular force between the surfaces exists. This attractive force produces a ®nite contact radius such that there is an energy balance between the released surface energy and the stored elastic energy around the interface, as shown in Fig. 8(b). The loss in free surface energy E_s is given by

$$E_s=-\pi a^2\Delta\gamma. \tag{4}$$

The attractive force F_s associated with this energy change is

$$F_s=-dE_s/d\delta, \tag{5}$$

where δ is the normal movement of the bodies, given by the Hertz equations[3,4] as $\delta=a^2/R$. Combining Eqs. (4) and (5) with the Hertz equations, we get

$$F_s=\pi R\Delta\gamma. \tag{6a}$$

From Hertz analysis the contact radius at no externally applied force is

$$a=\left(\frac{3F_sR}{4E^*}\right)^{1/3}, \tag{6b}$$

where R is the composite radius and E^* is the composite modulus.

This theory is approximate since contact stresses, even in the enlarged area, are assumed to be Hertzian. However, when spherical surfaces are maintained in contact over an enlarged area by surface forces, the stresses between the surfaces are tensile at the edge of the contact area (peripheral region) and only remain compressive in the center; see Fig. 8(c).[50] Since the applied force is zero, the integrated compressive force must equal the integrated tensile force. Furthermore, in the case of a sphere with relatively low elastic modulus, the deformed pro®le of the sphere outside the contact area is also changed. A determination of the contact equilibrium between elastic spheres under surface forces involves computation of the total energy in the system, including surface energy effects, as a function of contact radius.[50] Based on the modi®ed Hertz analysis, referred to as JKR analysis, expressions, for a tensile force F_s required to pull spheres apart and the residual contact radius a when the external load is reduced to zero, are

$$F_s=\tfrac{3}{2}\pi R\Delta\gamma \tag{7a}$$

and

$$a=\left(\frac{9\pi\Delta\gamma R^2}{2E^*}\right)^{1/3}. \tag{7b}$$

Note that F_s is independent of elastic modulus. The value of F_s is the same whether the surfaces are initially pressed together with an external force or not. As a result of surface forces, contact size is larger than the Hertzian value without adhesion and will be ®nite for zero external force.

If we pull the spheres apart, the smallest force will begin to produce separation at the periphery of the contact region (where the forces are already tensile); the separating force will rapidly increase until a critical value is reached at which the rate of release of stored elastic energy just exceeds the rate of increase of surface energy arising from creation of free surface at the interface. The surfaces will then pull apart. The analysis predicts that at zero applied force, the contact area and attractive force between the two spheres is ®nite, and they decrease as the applied force is made negative until a point is eventually reached at which the surfaces separate.

Experimental data of the contact zone formed between a rubber sphere and a rubber ¯at as the initial joining load of 4 g is gradually reduced and then made negative, is shown in Fig. 9. The contact radius a remains ®nite until a critical tensile force of about -0.75 g is reached. Then it suddenly

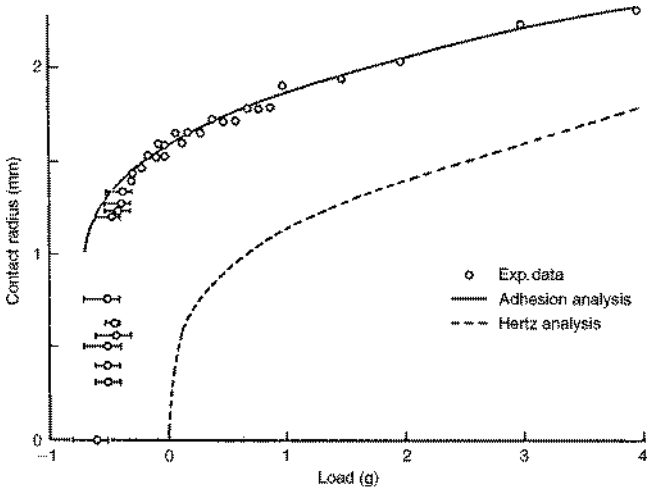

FIG. 9. Radius of contact zone formed between a rubber sphere (22 mm radius) and a rubber ¯at as the initial joining load of 4 g is gradually reduced and then made negative (Ref. 50).

falls to zero as the surfaces pull apart. Assuming a surface energy of rubber of about 34 mJ/m^2 for each rubber surface, agreement between the theory and data is very good. Hertz analysis does not predict this behavior.

Another analysis was developed by Derjaguin, Muller, and Toporov[51] (DMT analysis) for a sphere with high elastic modulus whose pro®le does not change outside the contact area. The contact region is under compression with the Hertzian distribution of stresses. For negligible elastic deformation of the sphere on a rigid surface, an expression for the tensile force required to pull spheres apart due to surface energy effects is given by

$$F_s = 2\pi R \Delta\gamma. \tag{8}$$

This equation is similar to Eq. (7) but has a coef®cient of 2 instead of 3/2. This equation is the same as that derived by Bradley.[48] The interaction of the surfaces was assumed to be governed by a Lennard-Jones potential by Muller *et al.*,[52,53] which corresponds to an attractive pressure as a function of distance between the two surfaces and energy of adhesion $\Delta\gamma$. It is known that the surface forces are of a reversible nature in equilibrium.

These analyses are recognized to apply to the opposite end of a spectrum of a nondimensional parameter:[54]

$$\theta = \left[\frac{R(\Delta\gamma)^2}{E^{*2} z_0^3}\right]^{1/3}, \tag{9}$$

where z_0 is the equilibrium spacing between two half-spaces made up of Lennard-Jones 6-12 particles and modeled as a continuum. The parameter θ is a measure of the magnitude of the elastic deformation compared with the range of surface forces. For small θ (say less than 0.1) elastic deformation is negligible (hard solids) and the DMT analysis provides a good approximation; for large θ (greater than 5 say), elastic deformation is large (soft solids) and the JKR theory is good. A useful analysis of the intermediate range has been developed by Maugis.[15,55]

The aforementioned analyses include two simplifying assumptions. First, that the surfaces are so smooth that they make molecular contact over the whole of the region. If the surfaces are initially of optical quality and if the modulus of the rubber is very low, small protrusions are easily squeezed down to a common level and this assumption becomes reasonably valid. This is probably one of the reasons why very soft rubbers generally appear to be tacky. If the surfaces are rough and/or hard, true molecular contact will occur over a smaller area within the macroscopic region. Second, it is assumed that the deforming solids are ideally elastic.

We now extend the analysis of a sphere against a ¯at rough surface in elastic contact. In an interaction between elastic solids, elastic energy is stored in the asperities as they deform to bring surfaces into intimate contact. If this elastic energy is signi®cant compared to the released surface energy ($\Delta\gamma$), the reduction in free energy is small and the resulting adhesion is small and vice versa. Fuller and Tabor[56] modeled asperity contacts of two rough surfaces using a statistical contact model. Their analysis predicts that the adhesion expressed as a fraction of maximum value (relative pull-off or adhesive force) depends upon a single parameter, called the adhesion parameter α, which is de®ned as

$$\alpha = \left(\frac{4\sigma_p}{3}\right)\left[\frac{E^*}{\pi R_p^{1/2}\Delta\gamma}\right]^{2/3}, \tag{10a}$$

where σ_p is the composite standard deviation of the summit heights, and R_p is the composite of mean radii of curvature of the summits of the two interacting surfaces.[3,4] The physical signi®cance of the parameter α can be seen by considering

$$\alpha^{3/2} = \frac{1}{\pi}\left(\frac{4}{3}\right)^{3/2}\frac{E^*\sigma_p^{3/2}R_p^{1/2}}{R_p\Delta\gamma}. \tag{10b}$$

We note that the denominator of Eq. (10b) is a measure of the adhesive force experienced by spheres of radius R_p and the numerator of Eq. (10b) is a measure of the elastic force needed to push spheres of radius R_p to a depth of σ_p into an elastic solid of modulus E^*. Clearly, the adhesion parameter represents the statistical average of a competition between the compressive forces exerted by the higher asperities that are trying to separate the surfaces and the adhesive forces between the lower asperities that are trying to hold the surfaces together. The relative pull-off (adhesive) force is virtually independent of initial applied load, and is a function solely of the adhesion parameter, as shown in Fig. 10(a). When the adhesion parameter is small (less than 1) the adhesive factor dominates and the adhesion is high, and it is small if the adhesion parameter is large (2 or greater).

Relative pull-off forces measured between optically smooth rubber spheres of various moduli and a hard ¯at surface of Perspex of various roughnesses are shown in Fig. 10(b). The data show that an increase in surface roughness that is small compared with the overall deformation occurring at the interface can produce an extremely large reduction in adhesion and the effect is more marked for rubbers of higher modulus. An increase in the modulus or a decrease in

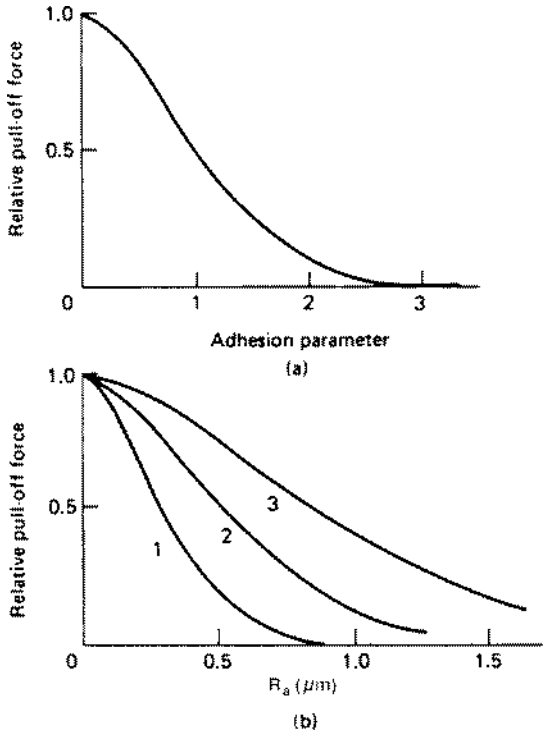

FIG. 10. (a) Predicted relative pull-off force as a function of the adhesion parameter (α) and (b) relative pull-off force for smooth rubber spheres in contact with a flat Perspex surface as a function of the R_a roughness of the Perspex for three moduli of the rubber: curve 1, 2.4 MPa; curve 2, 0.68 MPa; curve 3, 0.22 MPa. The pull-off force of smoothest surface was a few mN (Ref. 56).

the released surface energy also decreases the adhesion. On the other hand, the curvature of the sphere (over the range examined) had little influence. These results are consistent with the predictions of the analytical model [Fig. 10(a)].

For smooth and clean surfaces, the attractive forces can be on the order of several grams. In normal circumstances, the adhesion observed between hard solids when placed in contact is very small. This may be due either to surface films of low surface energy and/or surface roughness.

7. Chemical effects in adhesion and friction

The adhesion and friction of transition metals (metals with partially filled *d* shells) can be correlated with their relative chemical activity. The latter can be ascertained from their percentage of the *d*-bond character. The greater the percentage of the *d*-bond character, the less active the metal, and the lower is the adhesion and friction.[2,57]

8. Grain-boundary effects in adhesion

For polycrystalline materials, the presence of grain boundaries in the material influences adhesion, friction, and wear. The near surface dislocations in the sliding process are blocked in their movement by a grain boundary, they accumulate at the grain boundary and produce strain hardening in the surfacial layers. This strain hardening makes it more difficult for sliding and increases the friction force of materials in sliding contact.[2]

Strained metal, that is, metal that contains a high concentration of dislocations, is chemically more active on the surface because the presence of defects increases the energy in the material.[14,29,58] A grain boundary is a strained condition in that there are a large number of dislocations present to help accommodate the misfit or mismatch in adjacent orientations plus there are rows of strained atoms that must help in accommodating the mismatch. Consequently, these regions are high-energy regions at the surface. The energy is greater at the boundary, and the boundary has its own characteristic energy that is separate and distinct from the energy of the grains on either side of the boundary.

Sliding friction experiments have been conducted by Buckley[58] and Weick and Bhushan[59] across the surface of grain boundaries to measure the influence of the grain boundary on friction. They have reported a marked change in friction value in the grain boundary region as compared to that in the grain.

9. Polymer adhesion

Polymeric solids are used in many industrial applications where inherently low adhesion, friction, and wear is desired. Interaction of polymeric solids primarily results in van der Waals attraction.[12,14,60] There are other factors involved with polymers. First, these materials are easily deformed by comparison with the other hard solids. With soft rubbers, for example, large areas of intimate contact can easily be established; consequently, although the interfacial forces themselves are weak, it is not difficult to obtain relatively high adhesive strengths. A similar factor probably accounts for the strong adhesion between sheets of thin polymeric films. Furthermore, being highly elastic solids, they can stretch appreciably under the influence of released elastic stresses without rupturing. Second, interdiffusion of polymeric chains across the interface may occur. This will greatly increase the adhesive strength, since valence bonds, as distinct from van der Waals bonds, will be established.[10] Third, for dissimilar materials, charge separation may lead to an appreciable electrostatic component.[13,38–41]

B. Liquid-mediated contact

Generally, any liquid that wets or has a small contact angle on surfaces will condense from vapor into cracks and pores on surfaces as bulk liquid and in the form of an annular-shaped capillary condensate in the contact zone; see Fig. 11. This spontaneous condensation and formation of adhesive bridges or menisci is due to the proximity of two surfaces and the affinity of these surfaces for condensing liquid. The presence of liquid films of the capillary condensates or pre-existing films of liquid can significantly increase the adhesion between solid bodies.[3–6]

Liquid-mediated adhesive forces can be divided into two components: a meniscus force due to surface tension and a rate-dependent viscous force. These forces increase for smaller gaps and smoother surfaces so that the adhesion of ultraflat surfaces can be extremely strong. Figure 12 shows schematically for a linear ramping load that the applied force

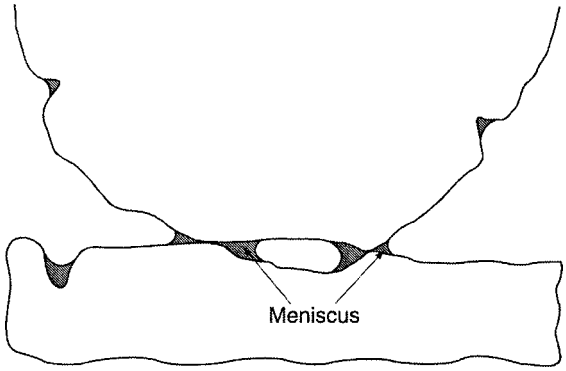

FIG. 11. Condensation from liquid vapor on the surfaces at the interface.

changes from meniscus to viscous before the surfaces are separated during a normal pull of the two surfaces. For an applied normal force less than the meniscus force there is no tendency for the surfaces to separate. When the force exceeds the meniscus force (F_m) at time t_m, then the viscous component in the normal direction ($F_{v\perp}$) is the excess over F_m. The force F_{ad} is the total required to separate the two surfaces in time t_s,

$$F_{\text{ad}}=F_m+F_{v\perp}. \tag{11}$$

The viscous component of the adhesive force is signi®cant for more viscous liquids (dynamic viscosity ~1 Pa s), but it can dominate for liquids of modest viscosity at high shear rates.

1. Idealized geometries

a. Meniscus forces. We study the effect of a liquid that wets, on the adhesion force between a macroscopic sphere and a surface and between two ¯at surfaces. In the former case, either a sphere can be in contact with a surface with a meniscus [Fig. 13(a)], can be close to a surface with a separation and with a meniscus [Fig. 13(b)], or can be close to a surface in the presence of a continuous ®lm and a meniscus forms on one of the surfaces [Fig. 13(c)].

Sphere on a plane surface. We ®rst consider the case of a sphere in contact with a plane surface with a meniscus [Fig. 13(a)]. If a liquid is introduced at the point of contact, the surface tension results in a pressure difference across a meniscus surface, referred to as capillary pressure or Laplace pressure. The pressure inside the liquid in a concave meniscus (Kelvin radius $r_K<0$) is lower than it is outside the liquid. (The inverse of the Kelvin radius is equal to the sum of the inverses of the meniscus curvatures r_1 and r_2 along the two mutually orthogonal planes. Note, $r_1 \gg r_2$.) If the liquid wets the (hydrophilic) surface ($0 \leqslant \theta < 90$É, where θ is the contact angle between the liquid and surface), the liquid surface is constrained to lie parallel with the surface, and the complete liquid surface must therefore be concave in shape. The exact geometric shape of the meniscus depends upon the liquid volume and its properties and on the interface geometry. The geometric shapes of the meniscus and meniscus force as a function of relative humidity, radius of the sphere, surface tension, and contact angles have been reported by Stifter *et al.*[61]

The attractive Laplace force for a sphere in contact with a plane surface is

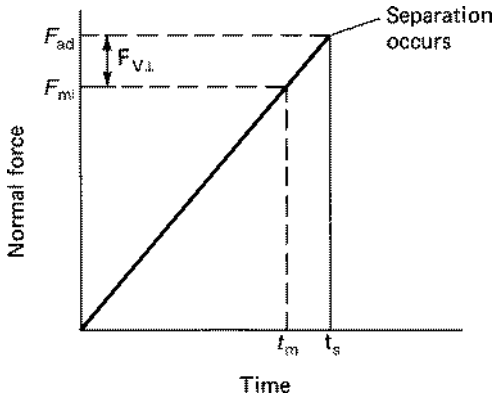

FIG. 12. Force±time relationship for a linearly ramping force during normal pull of two surfaces with a liquid bridge. The schematic shows the meniscus and viscous contributions.

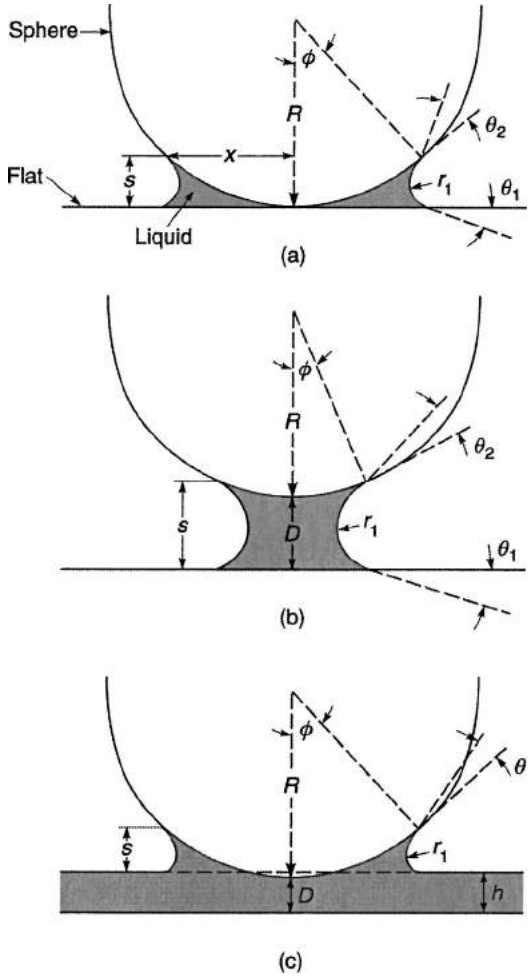

FIG. 13. Meniscus formation from a liquid condensate at the interface for (a) a sphere in contact with a plane surface, (b) a sphere close to a plane surface, and (c) a sphere close to a plane surface with a continuous ®lm.

$$F_L \sim 2\pi R\gamma_\ell(\cos\theta_1+\cos\theta_2) \tag{12a}$$

$$\sim 4\pi R\gamma_\ell\cos\theta \quad (\text{if } \theta_1=\theta_2), \tag{12b}$$

where γ_ℓ is the surface tension of liquid, and θ_1 and θ_2 are the contact angles of the liquid with surfaces 1 and 2, respectively. Note that F_L is independent of the amount of liquid at the interface. However, the full meniscus force is realized only provided the ®lm thickness exceeds the combined roughnesses of the contacting surfaces. Equation (12) has been experimentally veri®ed by McFarlane and Tabor[34] and others. Israelachvili[6] has reported that meniscus force expression is valid for water meniscus radii down to 2 nm.

Another component of the adhesive force arises from the resolved surface tension around the circumference. The normal component of the surface tension force is

$$F_T = 2\pi R\gamma_\ell \sin\phi \sin(\phi+\theta). \tag{13}$$

The F_T component is always small for small ϕ compared to the Laplace pressure contribution except for large θ close to 90É (when $\cos\theta\sim 0$) as well as for large ϕ. The angle ϕ is generally small in asperity contacts. However, menisci formed around ®ne particles interposed between two surfaces can result in high ϕ.[62] For most cases with small ϕ, the meniscus force,

$$F_m = F_L + F_T \sim F_L = 4\pi R\gamma_\ell\cos\theta. \tag{14}$$

Yet another adhesive force must be included in the preceding analysis. This arises from the direct solid±solid contact inside the liquid annulus; see Fig. 13(a). This force F_s is given by either Eq. (7a) or (8). Based on DMT analysis [Eq. (8)], for two identical solids of free surface energies in liquid γ_{sL} ($\Delta\gamma = 2\gamma_{sL}$) using Eq. (12b), the total adhesive force is

$$F_m = 4\pi R(\gamma_\ell\cos\theta+\gamma_{sL}). \tag{15}$$

Sphere close to a surface. For the case of a sphere close to a surface with a separation D and with a meniscus [Fig. 13(b)],[6]

$$F_L = \frac{2\pi R\gamma_\ell(\cos\theta_1+\cos\theta_2)}{(1+D/s)}. \tag{16}$$

This analysis is based on consideration of how the total free surface energy of the system changes with separation D. It is assumed that ϕ is small and liquid volume remains constant. Maximum attraction occurs at $D=0$, for which Eq. (16) reduces to Eq. (12).

Sphere close to a surface with continuous liquid ®lm For the case of a sphere close to a surface in the presence of a continuous liquid ®lm of thickness h and meniscus formed on the sphere [Fig. 13(c)],[63]

$$F_L = 2\pi R\gamma_\ell(1+\cos\theta), \tag{17}$$

where θ is the contact angle between the liquid and the sphere. The contact angle with the lower liquid ®lm is zero and Eq. (17) can be obtained from Eq. (12) by substituting $\theta_2=\theta$ and $\theta_1=0$. Note that for a ®nite value of ®lm thickness, F_L is independent of ®lm thickness.

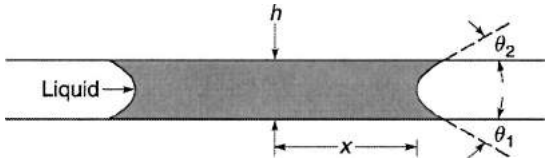

FIG. 14. Meniscus formation from a liquid condensate between two ¯at surfaces.

Two ¯at surfaces separated by a liquid ®lm For the case of two ¯at surfaces ($R\to\infty$) separated by a liquid ®lm of thickness h, $s=h$ and for projected area of the meniscus A_m comprising the liquid ®lm (Fig. 14), F_L is[3,4]

$$F_L \sim \frac{A_m\gamma_\ell(\cos\theta_1+\cos\theta_2)}{h}. \tag{18a}$$

Meniscus area can be less than or equal to the interfacial area of any shape. For a circular meniscus of radius x, $A_m = \pi x^2$, and

$$F_L = \frac{\pi x^2\gamma_\ell(\cos\theta_1+\cos\theta_2)}{h}. \tag{18b}$$

The meniscus forces can be large for two ¯at surfaces with large menisci.

An example of the effect of water vapor (relative humidity) on the adhesive force for a hemispherically ended pin of Ni±Zn ferrite in contact with a ¯at of Ni±Zn ferrite is shown in Fig. 15.[7] Note that the adhesive force remained low below about 60% relative humidity (RH); it increased greatly with increasing relative humidity above 60%. The adhesion at saturation is 30 times or more greater than that below 80%

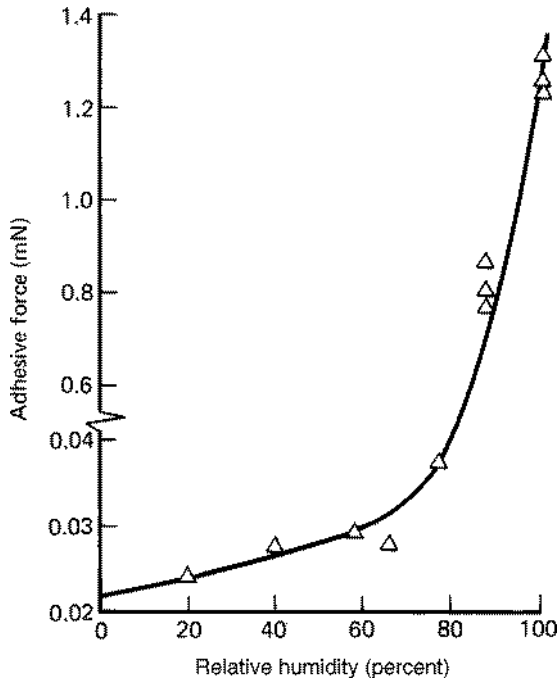

FIG. 15. Effect of humidity on adhesion of a hemispherically ended pin of 2 mm radius of Ni±Zn ferrite in contact with a ¯at of Ni±Zn ferrite in nitrogen atmosphere in the load range of 0.67±0.87 mN (Ref. 7).

RH. The change in the adhesive force of contacts was reversible on humidifying and dehumidifying. Adhesion was independent of the normal load (in the range studied). Adhesive force measured in saturated atmosphere of 1.35 mN can be predicted using meniscus analysis of sphere-¯at contact. This shows that the increase in adhesion of ferrite against itself at increasing humidity primarily arises from the meniscus (surface tension) effects of a thin ®lm of water adsorbed in the interface.

b. Viscous forces Based on experimental evidence, the viscous component of the adhesive force for a liquid-mediated contact is given by[34]

$$F_v = \frac{\beta \eta_\ell}{t_s}, \tag{19}$$

where β is a proportionality constant (dimension of length^2), η_ℓ is the dynamic viscosity of the liquid, and t_s is the time to separate (unstick) the two surfaces. We note that t_s is inversely related to acceleration or velocity of the interface during start-up. We further note that the ¯uid quantity has a weak dependence on the viscous force.

To overcome a viscous force, a critical viscous impulse I_v must be exceeded, de®ned by the time (t) integral of the viscous force,[2,64]

$$I_v = \int_{t_m}^{t_s} F_v dt. \tag{20}$$

I_v is independent of the rate at which the separation is performed. A constant applied force F_v is related to the separation time, t_s, from Eq. (20),

$$F_v = \frac{I_v}{t_s}. \tag{21a}$$

For a linearly ramping applied force $F_v = \dot{F}t$, we obtain the peak viscous force from Eq. (19),

$$F_v = (2\dot{F} I_v)^{1/2} \tag{21b}$$

and

$$\dot{F} = kV,$$

where $\dot{F}$ is the instantaneous rate of change of force and is proportional to the velocity V (constant velocity) and k is the stiffness of the loading member.

If the applied force accelerates at a constant rate (constant acceleration) $\ddot{F}$, then the peak viscous force is

$$F_v = \left(\frac{9}{2}\ddot{F} I_v^2\right)^{1/3} \tag{21c}$$

and

$$\ddot{F} = k\alpha,$$

where α is the start-up linear acceleration. Equations (21b) and (21c) show that the viscous force increases proportionally with the square root of the start-up velocity or cube root of the start-up acceleration for an interface that moves at constant velocity or constant acceleration (before separation), respectively. It is further assumed that separation occurs instantly at some critical value.

Equation (21) applies for any surface geometry separation along any path; geometry and path information are contained in the appropriate expression for I_v. It is readily shown that, assuming a zero contact angle, θ, the impulse, required to separate two ¯at surfaces bridged by a ¯uid ®lm of circular meniscus radius x and of thickness h (Fig. 14), in the perpendicular and parallel directions (required for calculation of friction to be described later) are

$$I_{v\perp} = \frac{3\pi \eta_\ell x^4}{8h^2}, \tag{22a}$$

$$I_{v\parallel} = \frac{16 \eta_\ell x^3}{3h}. \tag{22b}$$

The viscous impulse for sliding of a sphere over a ¯at [Fig. 13(a)] is not known but by analogy with the expressions for parallel plates and using an effective plate separation, an approximate expression for sliding of a sphere away from the wetting zone is given as[64]

$$I_{v\perp} = 6\pi \eta_\ell R^2 \ln\left(\frac{h}{2h_m}\right), \tag{23a}$$

$$I_{v\parallel} = \frac{32}{3}\eta_\ell R(Rh)^{1/2} \ln\left(\frac{2h}{h_m}\right), \tag{23b}$$

where h_m is the distance of the closest approach of the asperity and the ¯at surface, which could be interpreted as the microroughness of the asperity or the size of ¯uid molecule, and h is the average (original) thickness of the liquid ®lm.

For two ¯at surfaces of area A_a of any geometry, bridged by a ¯uid ®lm and not separating instantly, the peak viscous force for constant acceleration is given by[65]

$$F_{v\parallel} = \frac{\eta_\ell A_a}{h}(L\alpha)^{1/2} \exp(-1/2), \tag{24}$$

where L is the distance surfaces slide to become unstuck.

c. Kinetic meniscus analysis. So far, we have discussed meniscus forces at equilibrium. When a body ®rst comes in static contact (or rest) on another body, in the presence of liquid ®lm, the interface is not in equilibrium. The ¯ow of liquid results in an increase in the wetted meniscus area which causes an increase in the meniscus force until it reaches equilibrium.[3,4,66] This explains the experimentally observed increase in adhesive force with rest time in a liquid-mediated contact.[2±4,8]

2. Multiple-asperity contacts

Consider a smooth surface on a rough surface. Figure 16 shows a model of the contact region with different levels of ®lls of the interface dependent upon the mean interplanar separation and the liquid levels. Four distinct regimes are shown.[1,2±4,67] In the ®rst three regimes, menisci are formed which contribute to meniscus forces. The ®rst and third are the extreme regimes in which either a small quantity of liq-

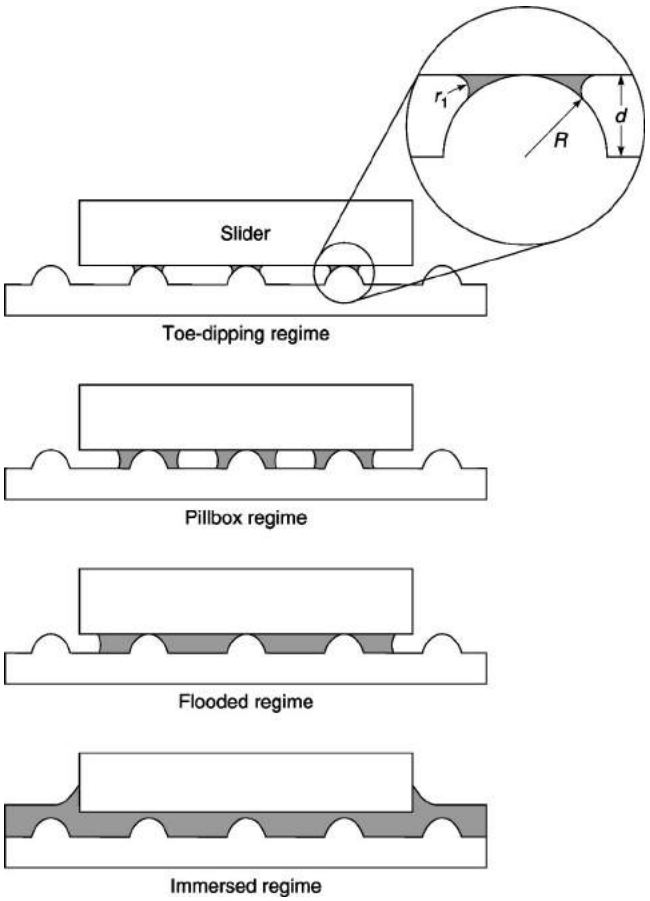

FIG. 16. Regimes of different liquid levels at the interface with a smooth slider surface in contact with a rough surface.

uid bridges the surfaces around the tips of contacting asperities (the ``toe-dipping" regime ) or the liquid bridges the entire surface (the ``¯ooded" regime) and in the second regime (the ``pillbox" regime ), the liquid bridges the surface around one or more asperities to a large fraction of the apparent area. The ¯ooded regime has the potential of generating very high adhesive forces. In the fourth regime (the ``immersed" regime), the interface is immersed in the liquid and thus meniscus forces do not exist. Only viscous forces are present.

For a suf®ciently thin liquid ®lm, $r_1 < d/2$ (d=interplanar separation), the contacting surfaces will be in the toe-dipping regime. For a suf®ciently thick ®lm so that the equilibrium Kelvin radius is greater than half the interplanar separation d, the menisci will form pillbox-shaped cylindrical menisci with a capillary radius $r_1 > d/2$ around the contacting asperities. These pillbox menisci, which initially have an attractive Laplace pressure higher than the disjoining pressure in the lubricant ®lm, grow by draining the surrounding lubricant ®lm until it is thin enough to have a disjoining pressure equal to the Laplace pressure, $p_L = 2\gamma_\ell / d$. The pillbox regime, however, is thermodynamically unstable, as the liquid ®lm away from the interface has its original thickness and low disjoining pressure. Consequently, the high attractive Laplace pressure of the pillboxes will slowly pull in liquid from the ®lm on the surface surrounding the contact regions, until the interface ®rst becomes ¯ooded, then immersed, and the appropriate equilibrium meniscus radius can form along the sides of the body.

In the toe-dipping regime, the liquid adhesion force between a single asperity and a surface can be modeled by a sphere of composite radius of curvature in contact with a ¯at surface, with a liquid bridge in between. Total meniscus and viscous forces of all wetted asperity contacts can be calculated by multiplying the number of contacts by meniscus and viscous forces at a typical contact. The ¯ooded regime can be modeled by a liquid bridge between two ¯at surfaces. Note that in the toe-dipping regime, the meniscus force is independent of the apparent area and proportional to the normal load (i.e., the number of asperity contacts). However, the ¯ooded regime shows the opposite tendencies. The pillbox regime is intermediate and can exhibit either behavior at the extremes. Meniscus force generally decreases with an increase in roughness σ.

If one assumes that surface asperity radii are constant and their heights follow a Gaussian distribution, the true coef®cient of friction μ_r can be obtained from the following expressions for the friction forces for the two regimes.[2]

For the toe-dipping regime:

$$F \sim \frac{\mu_r W}{1-[16.6\gamma_\ell(\cos\theta_1+\cos\theta_2)]/[E^*\sigma_p(\sigma_p/R_p)^{1/2}]}. \tag{25}$$

For the ¯ooded regime:

$$F = \mu_r\left[W + \frac{A_a\gamma_\ell}{h}(\cos\theta_1+\cos\theta_2)\right] + \frac{\eta_\ell A_a}{h}(L\alpha)^{1/2} \times \exp(-1/2), \tag{26a}$$

where

$$h/\sigma_p \sim 1.4\{\log[0.57R_p\sigma_p E^*(\sigma_p/R_p)^{1/2}/p_a]\}^{0.65} \tag{26b}$$

and p_a is the apparent pressure, E^* is the composite elastic modulus, and σ_p and R_p are the composite standard deviation and mean radius of curvature of asperity summits, and η is the summit density.

a. Statistical analysis of contacts. A schematic of a random rough surface in contact with a smooth surface with a continuous liquid ®lm on the smooth surface is shown in Fig. 17. Note that both contacting and near-contacting asperities wetted by the liquid ®lm contribute to the total meniscus force. A statistical approach is used to model the contact. The peak heights are assumed to follow a Gaussian distribution function and peak radii are assumed to be constant. In general, given the peak-height distribution function $p(z)$, the mean peak radius (R_p), the thickness of liquid ®lm (h), the liquid surface tension (γ_ℓ), and the contact angle for the liquid in contact with the rough surface (θ), the total meniscus force (F_m) at the sliding interface is obtained by summing up the meniscus forces from all individual contacting and noncontacting asperities that form menisci over the nominal contact area $[(F_m)_i]$ shown in Fig. 17.[63] For the surface height distribution considered here, peak radii of

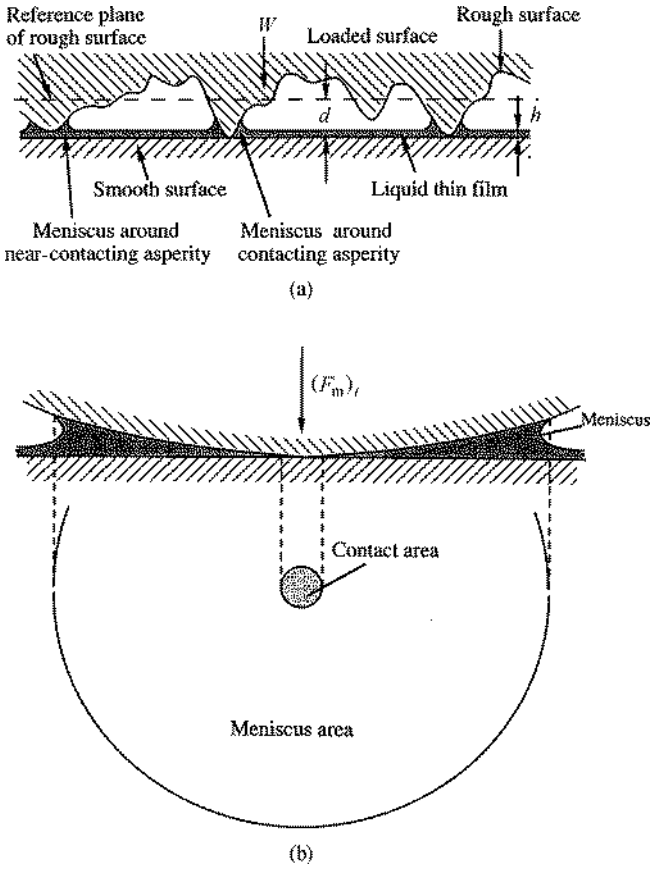

FIG. 17. (a) Schematic for a rough surface in contact with a ¯at surface with a liquid ®lm, and (b) schematic of contact area and meniscus area in a contacting asperity.

various contacts are the same, consequently, meniscus contribution of each contact is the same. The total meniscus force is given as

$$F_m = 2\pi R_p \gamma_\ell (1+\cos\theta) N \int_{d-h}^{\infty} p(z)dz, \tag{27}$$

where N is the total number of peaks in the nominal contact area. The interplanar separation, d, is determined from[63]

$$W + F_m = \frac{4}{3} E^* R_p^{1/2} N \int_d^{\infty} (z-d)^{3/2} p(z)dz. \tag{28}$$

An iterative numerical approach is used to solve Eqs. (27) and (28).

It is evident that the maximum meniscus force can be obtained by setting h very large so that the integral in Eq. (27) approaches its maximum value of unity. Therefore the maximum possible mensicus force is

$$F_{\max} = 2\pi R_p \gamma_\ell (1+\cos\theta) N \tag{29}$$

regardless of the distribution function of peak heights. Conversely, when the ®lm thickness$h$ is very small, i.e., less than a molecular layer thick, F_m is zero since no meniscus can be formed and the problem reduces to dry contact.

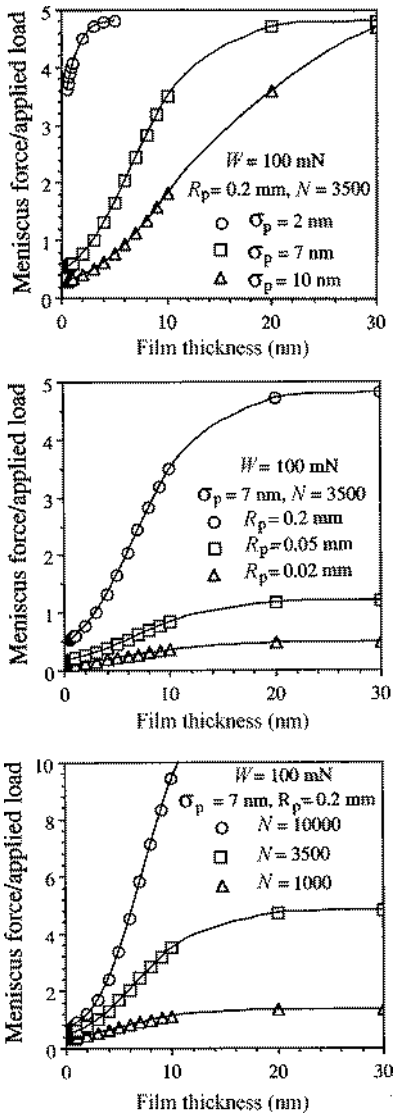

FIG. 18. Ratio of the meniscus force to applied load (F_m/W) as a function of water ®lm thickness at different σ_p, R_p, and N for an interface (Ref. 63).

Meniscus force increases as a function of liquid ®lm thickness (h). For a given ®lm thickness, meniscus force decreases with an increase in standard deviation of peak heights (σ_p) and it increases with an increase of radii of peaks (R_p) and number of peaks (N), Fig. 18.

It has been reported that non-Gaussian surfaces with a range of positive skewness (between 0.3 and 0.7) and a high kurtosis (greater than 5) exhibit low real area of contact and meniscus forces and these surfaces are somewhat insensitive to liquid ®lm as far as magnitude of meniscus force is concerned.[68] Further discussion will be presented in the next section.

b. Numerical three-dimensional contact models. In a numerical model, meniscus forces as a result of multi-asperity contacts with a pre-existing liquid ®lm during contact of two rough surfaces are calculated. The meniscus force due to the Laplace pressure is given by[69]

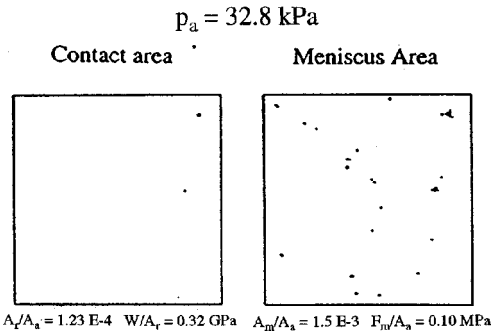

FIG. 19. Contact area and meniscus area for the case of computer-generated rough surface (σ=1 nm, β^*=0.5 μm) in contact with a smooth surface with a composite elastic modulus of 100 GPa and a nominal pressure (p_a) of 32.8 kPa, in the presence of water ®lm (γ_ℓ=73 dyn/cm, θ=60É) thickness of 1 nm and meniscus height of 1 nm.

$$F_m = \int\int_{\Omega} p_L(x,y)\,d\Omega$$

$$= \gamma_\ell \int\int_{\Omega} \frac{1}{r_1}\,d\Omega \sim \gamma_\ell(\cos\theta_1 + \cos\theta_2)\frac{\Omega}{\bar{A}}, \qquad (30)$$

where p_L is the Laplace pressure, r_1 is the meniscus radius, $\bar{A}$ is the mean meniscus height, and Ω is the projected area of meniscus enclave which intersects the upper contacting asperity at a mean meniscus height. For multiple isolated menisci scattered over the whole contact interface, Ω should be the sum of the projected area of each meniscus enclave. To solve Eq. (30), we need to know both the meniscus radius at different locations (or mean meniscus height) and the projected area of the meniscus enclave. These parameters are a function of the shape and the size of the meniscus.

In the numerical wet model developed by Tian and Bhushan,[69] elastic-plastic dry contact of rough surfaces[3,4] is ®rst analyzed. In the next step, a liquid ®lm of known mean thickness is introduced over the deformed rough surfaces. Wetted areas are determined by selecting the areas where asperities of both contacting surfaces touch the liquid. A mean meniscus height is assumed, Ω is calculated, and Eq. (30) is used to calculate the meniscus force. Figure 19 shows representative contact area and meniscus area maps for a computer-generated rough surface in contact with a smooth surface in the presence of water ®lm. As expected, the meniscus area is larger than the contact area and the meniscus force is three times that of the normal force. The number and size of contacts increase with an increase in the apparent contact pressure. The effect of relative humidity on an interface is shown in Fig. 20(a). The effect of liquid ®lm thickness and interface roughness on meniscus force for computer-generated rough surfaces in contact with a smooth surface is shown in Fig. 20(b). An increase in either relative humidity or liquid ®lm thickness increases the liquid present at the interface. The thicker a liquid ®lm, the more asperities touch the liquid surface and the larger the number of asperities on which menisci form. In addition, with a thicker ®lm,

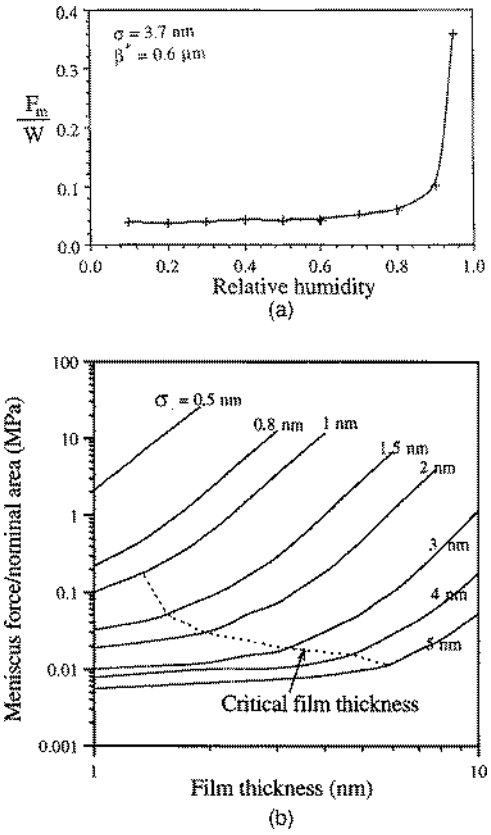

FIG. 20. (a) Effect of relative humidity on the relative meniscus force for a glass ceramic disk substrate in contact with a smooth surface, and (b) the effect of water ®lm thickness and surface roughness on the relative meniscus force for computer generated Gaussian surfaces (correlation distance β^*=0.5 μm) in contact with a smooth surface. The dotted line de®nes the critical ®lm thickness for different σ (Ref. 116).

a larger volume of liquid is present around the asperities, resulting in a greater amount of meniscus volume accumulated at the contact interface and in a greater meniscus height. These effects lead to larger meniscus forces. There is a critical ®lm thickness for a surface with given roughness, above which the meniscus force increases rapidly. The critical ®lm thickness is on the order of three-quarters of the liquid ®lm thickness. Experimental evidence for these observations will be presented later.

Selected non-Gaussian surfaces exhibit low real area of contact. Figure 21 shows the probability density functions of non-Gaussian surfaces with various skewness (Sk) and kurtosis (K) values. The three-dimensional contact model has been used to study the effect of skewness and kurtosis on real area of contact and meniscus forces.[70±72] Figure 22(a) shows the effect of skewness and kurtosis on the fractional real area of contact (A_r/A_a, where A_a is the apparent area) and the relative meniscus force (F_m/W) at different nominal pressures. A positive skewness between 0 and 0.2 at low pressure and about 0.2 at higher pressures results in the lowest real area of contact and meniscus force. Contact area and meniscus force decrease with an increase in the kurtosis. Fewer peaks present on a surface with positive skewness or high kurtosis can explain the trends. Figure 22(b) shows the

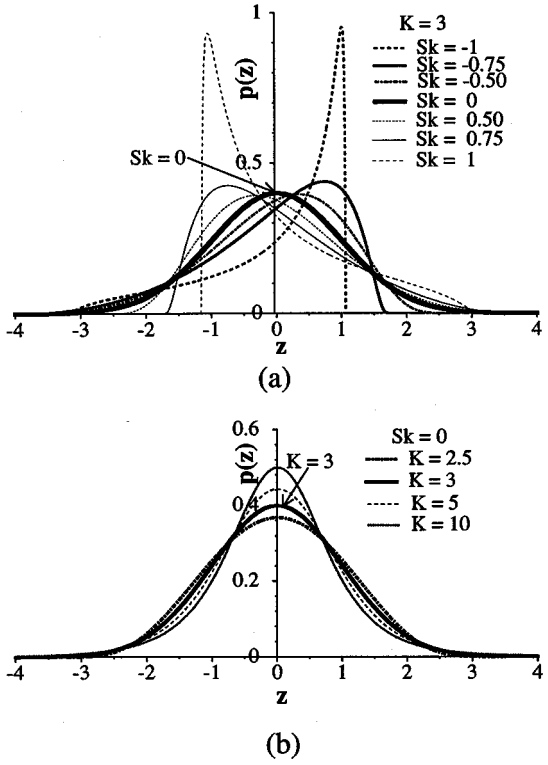

FIG. 21. Probability density functions for surfaces with (a) difference skewness (Sk) and (b) different kurtosis (K) values.

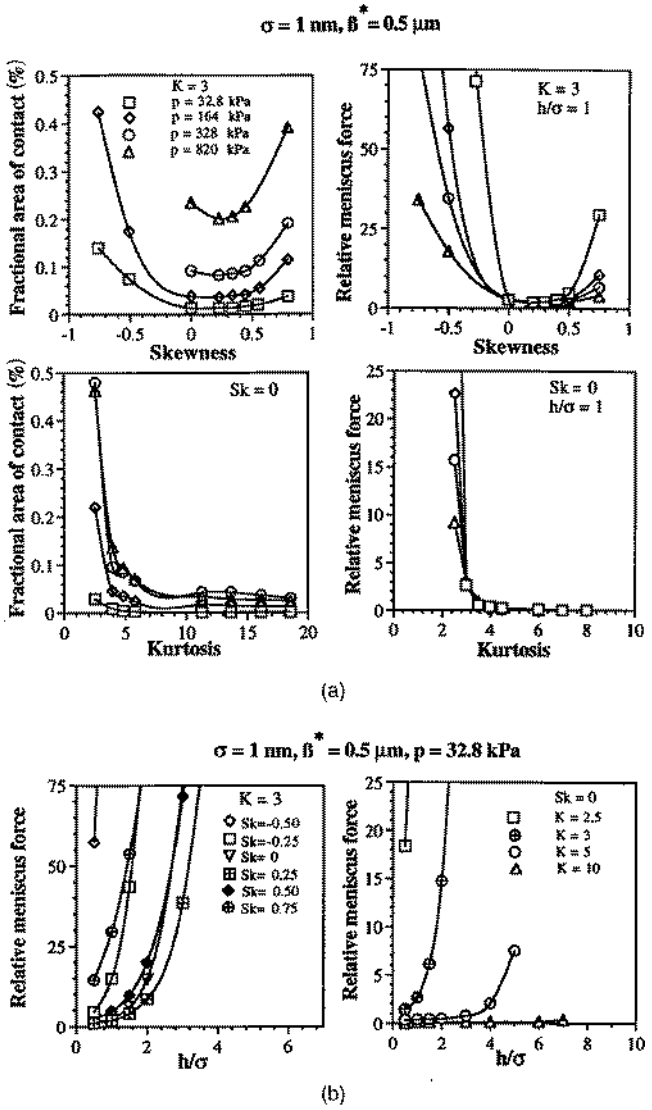

FIG. 22. (a) Fractional real area of contact and relative meniscus force as a function of skewness and kurtosis at various nominal pressures, and (b) relative meniscus force as a function of h/σ for different skewness and kurtosis values, for an interface in the presence of per¯uoropolyether liquid ®lm ($\gamma_\ell = 25$ dyn/cm, $\theta = 10$É).

variation of relative meniscus force with the h/σ ratio for different skewness and kurtosis values. Note that sensitivity of h/σ to meniscus force decreases at a range of positive skewness of 0 ± 0.2 and kurtosis values of about ®ve or larger are optimum.

C. Separation distance dependence of meniscus and van der Waals forces

When two hydrophilic surfaces come in close proximity in the presence of a liquid ®lm, they form a meniscus. The intrinsic attractive force always consists of meniscus and van der Waals (vdw) forces in addition to the result of some other sources, described earlier. As mentioned earlier, the magnitude of the meniscus force depends upon the liquid volume and its properties and on the interface geometry. Lower-surface tensions and larger contact angles can reduce the strength of the meniscus forces. The magnitude of weak vdw force depends on the Hamaker constants and the minimum separation distance between the two bodies. This force increases rapidly as the distance is reduced and can be large at a spacing of atomic dimensions.[2] In the case of two rough surfaces, the average interplanar distance would be large and the vdw forces would be small. However, these forces can be large for two smooth surfaces at a small separation distance.

If the two smooth surfaces under lightly loaded conditions are brought in close proximity, meniscus and vdw forces may be comparable to the external load, such as in scanning probe microscopy, magnetic storage devices, and MEMS/NEMS. The relative contribution of the two forces depends upon the separation distance among other things. Stifter *et al.* (2000)[61] studied the distance dependence of meniscus and vdw forces to study their relative importance at various operating conditions. They calculated vdw force as well as the Lennard-Jones force with the strongest vdw force. They considered a spherical body of radius R in contact with a ¯at surface in the presence of a liquid ®lm ($\gamma_\ell = 72.5$ N/m, $\theta_1 = \theta_2 = 0$É). For the meniscus analysis, the sphere was brought in contact with the mating surface and the meniscus was built and then the tip was retracted to a distance D.[61] Figure 23(a) shows the comparison of meniscus and vdw forces as a function of separation distance D. The two dashed curves in Fig. 23 indicate the spread of possible vdw forces. The dotted curve shows the Lennard-Jones force with the strongest van der Waals force. The two solid curves are meniscus forces at two relative humidities in terms of p/p_0, where p_0 is the normal

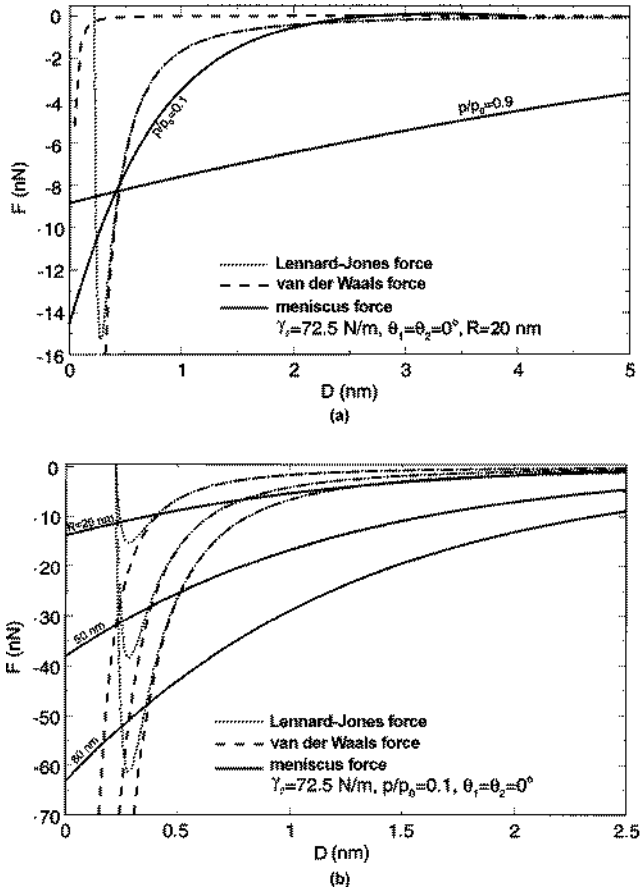

FIG. 23. Relative contribution of meniscus and van der Waals forces as a function of separation distance (D), (a) effect of relative humidity (p/p_0), and (b) sphere radius (R) (Ref. 61).

vapor pressure of the liquid and p is the pressure acting outside the curved surface. The meniscus force can be stronger or weaker than vdw force for distances smaller than about 0.5 nm. For greater distances, the meniscus force is stronger than the vdw force. vdw forces must be considered for a separation distance up to a few nanometers ($D<5$ nm). For many material combinations a smaller distance (<2 nm) is enough. Meniscus forces operate up to the break of the meniscus, ranging from 5 to 20 nm. Thus for large separations only the meniscus force is important while for smaller separations both forces must be considered.

Figure 23(b) shows the sphere radius dependence on both forces as a function of separation distance D for various values of radii.[61] The forces show an increase with an increase in radius. For the vdw force, the increase is exactly linear with the tip radius. The meniscus forces shown here are one of the strongest for each radius, together with the strongest van der Waals forces.

Based on the meniscus and vdw forces data presented in Fig. 23, three possible arrangements can occur. The meniscus force can be dominant, the vdw force can be dominant, or both forces can be roughly equal. vdw forces are generally dominant over a distance of 0.5±2 nm.

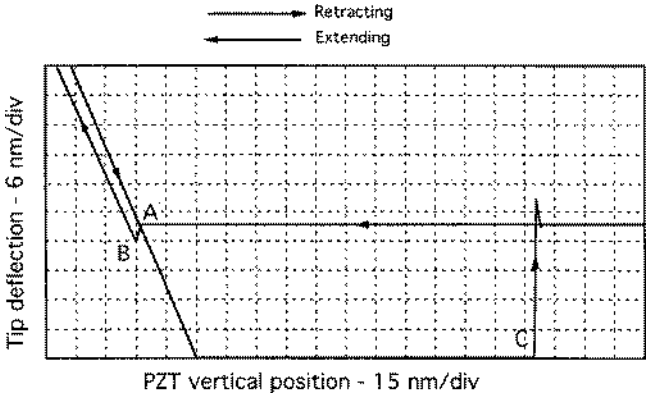

FIG. 24. Typical force±distance curve for a contact between Si_3N_4 tip and single crystal silicon surface in measurements made in the ambient environment. Contact between the tip and silicon occurs at point *B*; tip breaks free of adhesive forces at point *C* as the sample moves away from the tip.

III. ADHESION MEASUREMENT TECHNIQUES

A. Surface force apparatus and atomic force microscopy

Surface force apparatus (SFA) and atomic force microscopes (AFM) are used to measure adhesion on micro- to nanoscales between two surfaces. In the SFA, adhesion of liquid ®lms sandwiched between two curved smooth surfaces is measured. In an AFM, adhesive force measurement is performed in the so-called force calibration mode.[3,4,73] In this mode, force±distance curves are obtained, as shown for example in Fig. 24. The horizontal axis gives the distance the piezo (and hence the sample) travels and the vertical axis gives the tip de¯ection. As the piezo extends, it approaches the tip, which is at this point in free air and hence shows no de¯ection. This is indicated by the ¯at portion of the curve. As the tip approaches the sample within a few nanometers (point *A*), an attractive force exists between the atoms of the tip surface and the atoms of the sample surface. The tip is pulled toward the sample and contact occurs at point *B* on the graph. From this point on, the tip is in contact with the surface and as the piezo further extends, the tip is further de¯ected. This is represented by the sloped portion of the curve. As the piezo retracts, the tip goes beyond the zero de¯ection (¯at) line because of attractive forces (van der Waals forces and long-range meniscus forces), into the adhesive regime. At point *C* in the graph, the tip snaps free of the adhesive forces, and is again in free air. The horizontal distance between points *B* and *C* along the retrace line gives the distance moved by the tip in the adhesive regime. This distance multiplied by the stiffness of the cantilever gives the adhesive force. Incidentally, the horizontal shift between the loading and unloading curves results from the hysteresis in the PZT tube.[3,4,73,74]

B. Microtriboapparatus

To measure adhesion, friction, and wear between two microcomponents, a microtriboapparatus has been used. Figure 25 shows the schematic of a microtriboapparatus, capable of

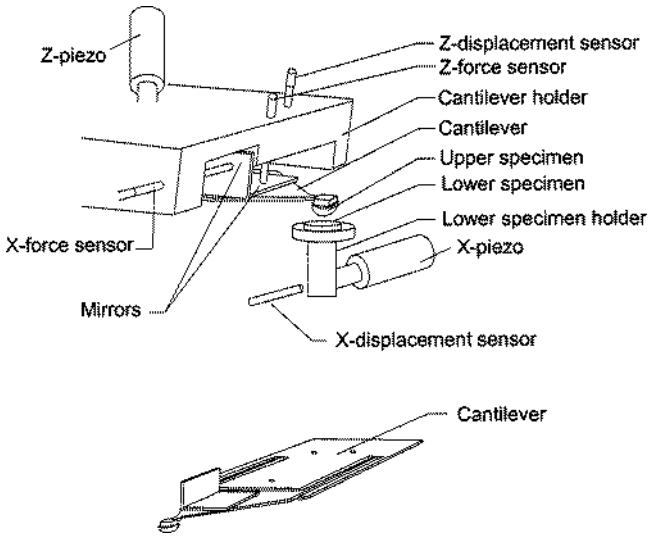

FIG. 25. Schematic of the microtriboapparatus including specially designed cantilever (with two perpendicular mirrors attached on the end), lower specimen holder, two piezos (X- and Z-piezos), and four ®ber optic sensors (X- and Z-displacement sensors and X- and Z-force sensors)ÐRef. 75.

adopting MEMS components.[75] In this apparatus, an upper specimen, mounted on a soft cantilever beam, comes in contact with a lower specimen mounted on a lower specimen holder. The apparatus consists of two piezos (X- and Z-piezos), and four ®ber optic sensors (X- and Z-displacement sensors, and X- and Z-force sensors). For adhesion and friction studies, Z- and X-piezos are used to bring the upper specimen and lower specimen in contact and to apply a relative motion in the lateral direction, respectively. The X- and Z-displacement sensors are used to measure the lateral position of the lower specimen and vertical position of the upper specimen, respectively. The X- and Z-force sensors are used to measure friction force and normal load/adhesive force between these two specimens, respectively, by monitoring the de¯ection of the cantilever.

C. Cantilever beam array technique

The propensity of adhesion between two surfaces can be evaluated by studying the tendency of microstructures with well-de®ned contact areas, covering a wide range of suspension compliances, to stick to the underlying substrate. The test structures, which have been used, include a cantilever beam array (CBA) with difference lengths[17,76±79] and stand-off multiple dimples mounted on microstructures with a range of compliances, free standing above a substrate.[80] The CBA technique, more commonly used, utilizes as array of micromachined polysilicon beams (for Si MEMS applications), in the mesoscopic length scale, anchored to the substrate at one end and with different lengths parallel to the surface. It relies on peeling and detachment of cantilever beams. Change in surface energy or reversible work done to separate unit areas of two surfaces from contact is called work of adhesion. To measure the work of adhesion, electrostatic actuation is used to bring all beams in contact with the substrate; see Fig. 26(a).[76±78] Once the actuation force is

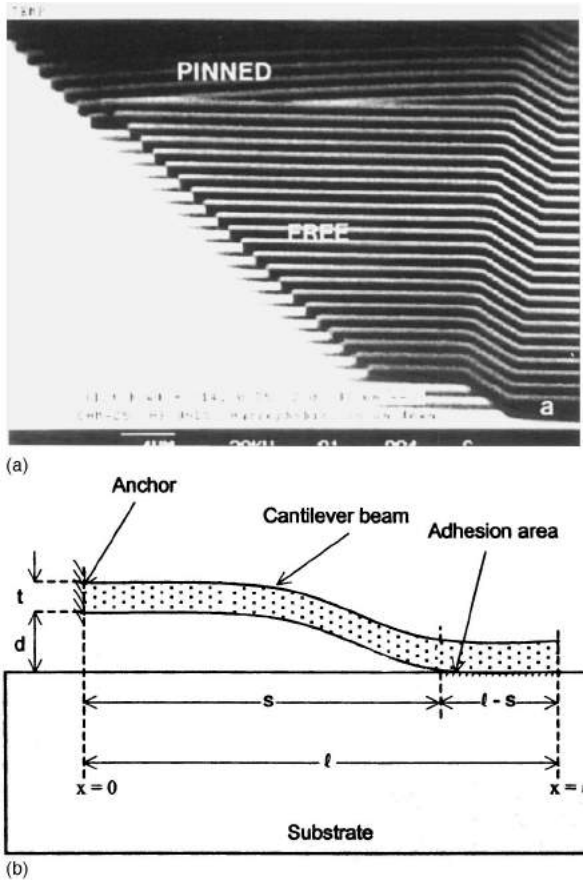

FIG. 26. (a) SEM micrograph of micromachined array of polysilicon cantilever beams of increasing length. The micrograph shows the onset of pinning for beams longer than 34 μm (Ref. 77), and (b) schematic of a cantilever beam of length ℓ adhering to its substrate in the presence of a liquid ®lm.

removed, the beams begin to peel themselves off the substrate. This can be observed with an optical interference microscope (e.g., Wyko surface pro®ler). For beams shorter than a characteristic length, the so-called detachment length, their stiffness is suf®cient to free them completely from the substrate underneath. Beams larger than the detachment length remain adhered. The beams at the transition region start to detach and remain attached to the substrate just at the tips. The technique has been used to screen methods for adhesion reduction in polysilicon microstuctures by using detachment length as a measure of work of adhesion.[76,77]

An expression for the work of adhesion as a function of detachment length is derived next.[76] Figure 26(b) shows a cantilever beam of length ℓ, thickness t, width w, and Young's modulus E, anchored at a spacing d. The beam attaches the underlying substrate at distance s from the anchor over a length $\ell \pm s$ from the tip. The stored elastic energy of the beam in the segment $0 \leqslant x \leqslant s$ induces a restoring force that tends to peel the beam from the adhering substrate. The adhesion energy stored in the segment $s \leqslant x \leqslant \ell$ induces another force that holds the beam in contact with the substrate. At equilibrium, the peel distance ℓ_d minimizes the total energy of the system (bending plus adhesion energies).

The elastic energy stored in the rectangular cantilever, using boundary conditions which allow the shear deformation of the tip of the beam,

$$U_E = \frac{Et^3 d^2 w}{8s^3}. \tag{31}$$

The interfacial adhesion energy stored in the attachment length $(\ell - s)$ is simply the work of adhesion per unit area, W_{ad}, times the area of contact

$$U_S = -W_{ad}(\ell - s). \tag{32}$$

The sign of work of adhesion is negative because it is a binding energy. The unit is $J\,m^{-2}$ or $N\,m^{-1}$. The total energy (or free energy) of the system is the sum of elastic plus adhesion energies. In equilibrium, the total energy is minimized and this gives the detachment length $(s^* = \ell_d)$,

$$\frac{d}{ds}(U_E + U_S) = 0. \tag{33}$$

Using expressions from Eqs. (31) and (32) into Eq. (33), one gets an expression for work of adhesion as a function of critical length of the cantilever beam or detachment length, ℓ_d. W_{ad} is given as

$$W_{ad} = \frac{3Et^3 d^2}{8\ell_d^4}. \tag{34}$$

IV. LUBRICATION APPROACHES AND TYPICAL STICTION DATA

Several studies on liquid per¯uoropolyether (PFPE) lubricant ®lms, self-assembled monolayers(SAMs), and hard diamondlike carbon (DLC) coatings have been carried out for the purpose of minimizing adhesion, stiction, friction, and wear.[3,4,19,75,81±88] Many variations of these ®lms are hydrophobic (low surface tension and high contact angle) and have low shear strength. These provide low adhesion, friction, and wear.

The classical approach to lubrication uses freely supported multimolecular layers of liquid lubricants.[3,4] The liquid lubricants are sometimes chemically bonded to improve their wear resistance. Partially chemically bonded, molecularly thick per¯uoropolyether (PFPE) lubricants (Z-DOL) are widely used for lubrication of magnetic storage media,[2] and are found to be suitable for MEMS/NEMS devices.[75,86,88,89]

A preferred method of lubrication of MEMS/NEMS is by the deposition of organized and dense molecular-scale layers of long-chain molecules, as they have been shown to be superior lubricants.[19,81,84±88] Two common methods to produce monolayers are the Langmuir±Blodgett (LB) deposition and self-assembled monolayers (SAMs) by chemical grafting of molecules. LB ®lms are physically bonded to the substrate by weak van der Waals forces while SAMs are bonded by covalent bonds to the substrate and provide high durability. SAMs can be spontaneously formed by immersion of an appropriate substrate into a solution of active surfactant in an organic solvent. SAMs offer the ¯exibility and advantage of molecular tailoring to obtain a variety of different tribological and mechanical properties. For example, researchers have shown that by changing the head groups, tail groups, chain lengths, or types of bonds within a chain, varying degrees of friction, adhesion, and/or compliance can be obtained.[85,87] These studies indicate that the basis for molecular design and tailoring of SAMs must include a complete understanding of interrelationships between the molecular structure and tribological properties of SAMs, as well as a deep understanding of the friction and wear mechanisms of SAMs at the molecular level.

Bhushan and Liu[85] and Liu and Bhushan[87] studied nanotribological properties of four different kinds of alkylthiol and biphenyl thiol monolayers with different surface terminals, spacer chains, and head groups using atomic force microscopy. They reported that compliant alkylthiolÐhexadecane thiol (HDT) ®lms exhibit superior adhesion, friction and wear resistance.

Hard amorphous carbon (*a*-C), commonly known as DLC (implying high hardness) coatings are deposited by a variety of deposition techniques including ®ltered cathodic arc, ion beam, electron cyclotron resonance chemical vapor deposition, plasma-enhanced chemical vapor deposition, and sputtering.[83] The coatings deposited by ®ltered cathodic arc deposition provide excellent friction and wear properties. DLC coatings are used in a wide range of applications including tribological, optical, electronic, and biomedical applications. Ultrathin coatings (3.5 to 10 nm thick) are employed to protect against wear and corrosion in magnetic storage applicationsÐthin-®lm-rigid disks, metal evaporated tapes, and thin-®lm read/write headÐ,Gillette Mach 3 razor blades, glass windows, and sunglasses. The coatings exhibit low friction, high hardness, and wear resistance, chemical inertness to both acids and alkalis, lack of magnetic response, and optical band gap ranging from zero to a few electron volts, depending upon the deposition technique and its conditions.

A number of adhesion and friction studies have been performed on DLC, chemically bonded Z-DOL, and HDT ®lms. Typical data follow.

A. Normal pull mode data

For two surfaces in the presence of liquid, intrinsic adhesive force may be large. It is well known that in computer rigid disk drives, the adhesive force increases rapidly with an increase in the rest time between a magnetic head and a magnetic disk.[2] Considering that the adhesion and friction are the major issues that lead to the failure of MEMS/NEMS devices, the rest time effect on micro- and nanoscales on Si(100), DLC, chemically bonded Z-DOL, and HDT have been studied by Liu and Bhushan[75] and Bhushan *et al.*[86] The results are summarized in Fig. 27. It is found that the adhesive force of Si(100) logarithmically increases with the rest time to a certain equilibrium time $(t = 1000\,s)$ after which it remains constant. Figure 27 also shows that the adhesive forces of DLC, Z-DOL, and HDT do not change with rest time. Single asperity contact modeling of the dependence of meniscus force on the rest time has been carried out by Chi-

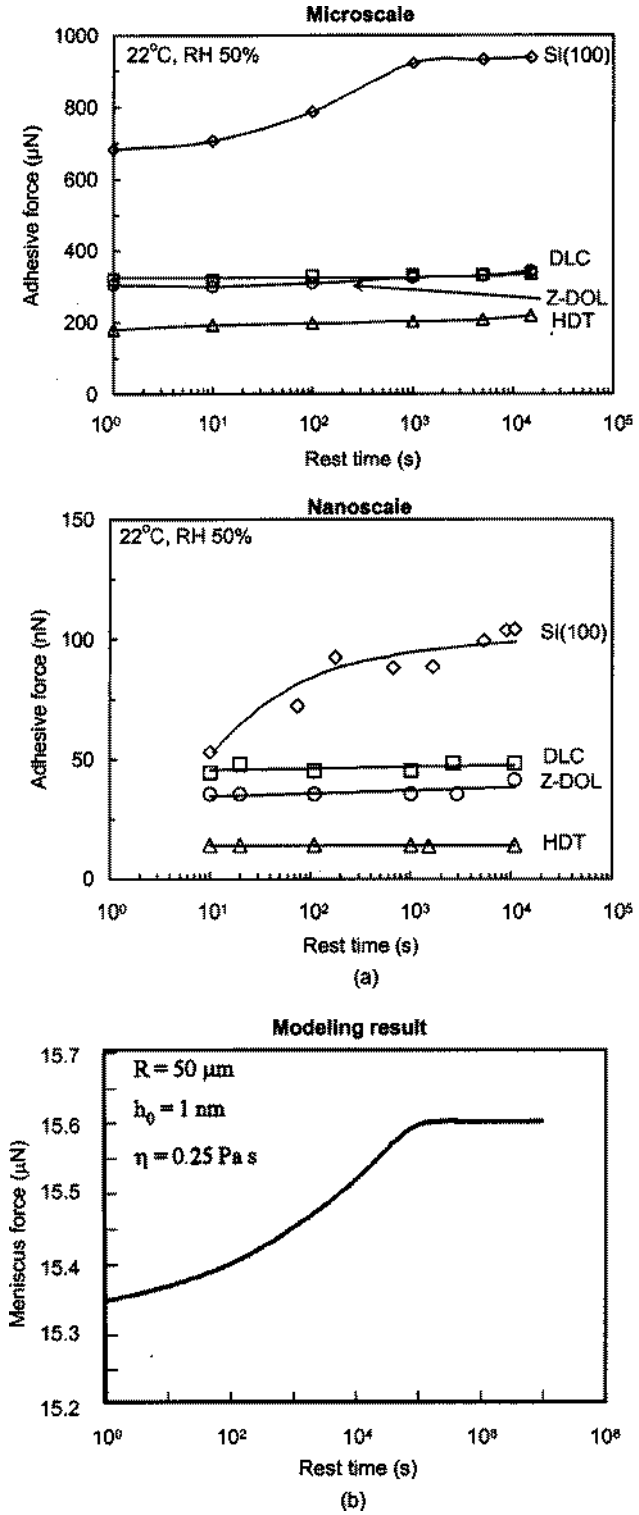

FIG. 27. (a) Influence of rest time on the adhesive force of Si(100), DLC, chemically bonded Z-DOL, and HDT, and (b) single asperity contact modeling results of the rest time effect on the meniscus force for an asperity of R in contact with a flat surface with a water film thickness of h_0 and absolute viscosity of η)–Ref. 66.

lamakuri and Bhushan,[66] and the modeling results (Fig. 27) verify experimental observations. Due to the presence of thin film adsorbed water on Si(100), menisci form around the contacting asperities and grows with time until equilibrium occurs, which causes the rest time effect on its adhesive force. The adhesive forces of DLC, Z-DOL, and HDT do not change with rest time which suggests that either the water menisci are not present on their surfaces or they do not increase with time.

The measured adhesive forces of Si(100), DLC, Z-DOL, and HDT at a rest time of 1 s on micro- and nanoscales are summarized in Fig. 28(a).[75,86] It shows that the presence of solid films of DLC, Z-DOL, and HDT greatly reduces the adhesive force of Si(100), whereas, HDT film has the lowest adhesive force. (It should be noted that contact pressures in the adhesion experiments are different for various samples because of differences in elastic properties, which will affect the magnitude of the adhesive forces.) It is well known that the native oxide layer (SiO_2) on the top of Si(100) wafer exhibits hydrophilic properties, and water molecules, produced by capillary condensation of water vapor from the environment, can easily be adsorbed on this surface. The condensed water will form meniscus as the upper specimen approaches to the lower specimen surface. The meniscus force is a major contributor to the adhesive force. For a simple case of a sphere in contact with a flat surface, the attractive Laplace force F_L caused by menisci is given by Eq. (12), presented earlier. In this study, the measured adhesive force on a microscale is generally higher than that measured on a nanoscale. This happens because the larger radius of the Si(100) ball, as compared to that of an AFM tip, induces larger F_L and van der Waals force. Figure 28(a) summarizes the measured contact angles of water against Si(100), DLC, Z-DOL, and HDT and the corresponding calculated Laplace forces F_L. The results show that DLC, Z-DOL, and HDT have larger contact angles, or in other words, lower surface energy than Si(100), which means that they exhibit more hydrophobicity.

The schematics in Fig. 28(b) show relative sizes of water meniscus on different specimens. Because DLC, chemically bonded Z-DOL, and HDT films have low free surface energy and can adsorb a small number of water molecules to form water meniscus, these films can reduce the adhesive force. The reason why the calculated F_L is smaller than the measured adhesive force is that in addition to F_L, van der Waals, electrostatic, and other possible surface forces also contribute to the adhesive force. These studies suggest that DLC, chemically bonded Z-DOL, and HDT films can act as antiadhesion films. They greatly reduce the adhesive force of Si(100) by modifying the surface hydrophobic property and can be applied in MEMS/NEMS.

B. Sliding mode data

The intrinsic attractive force due to liquid-mediated adhesion may result in high static friction, kinetic friction, and wear. The total normal force on the wet interface is the externally applied normal force plus the intrinsic meniscus force. Therefore, during sliding, in the absence of any hydrodynamic effects, the force required to initiate or sustain sliding is equal to the sum of the intrinsic (true) friction force F_i

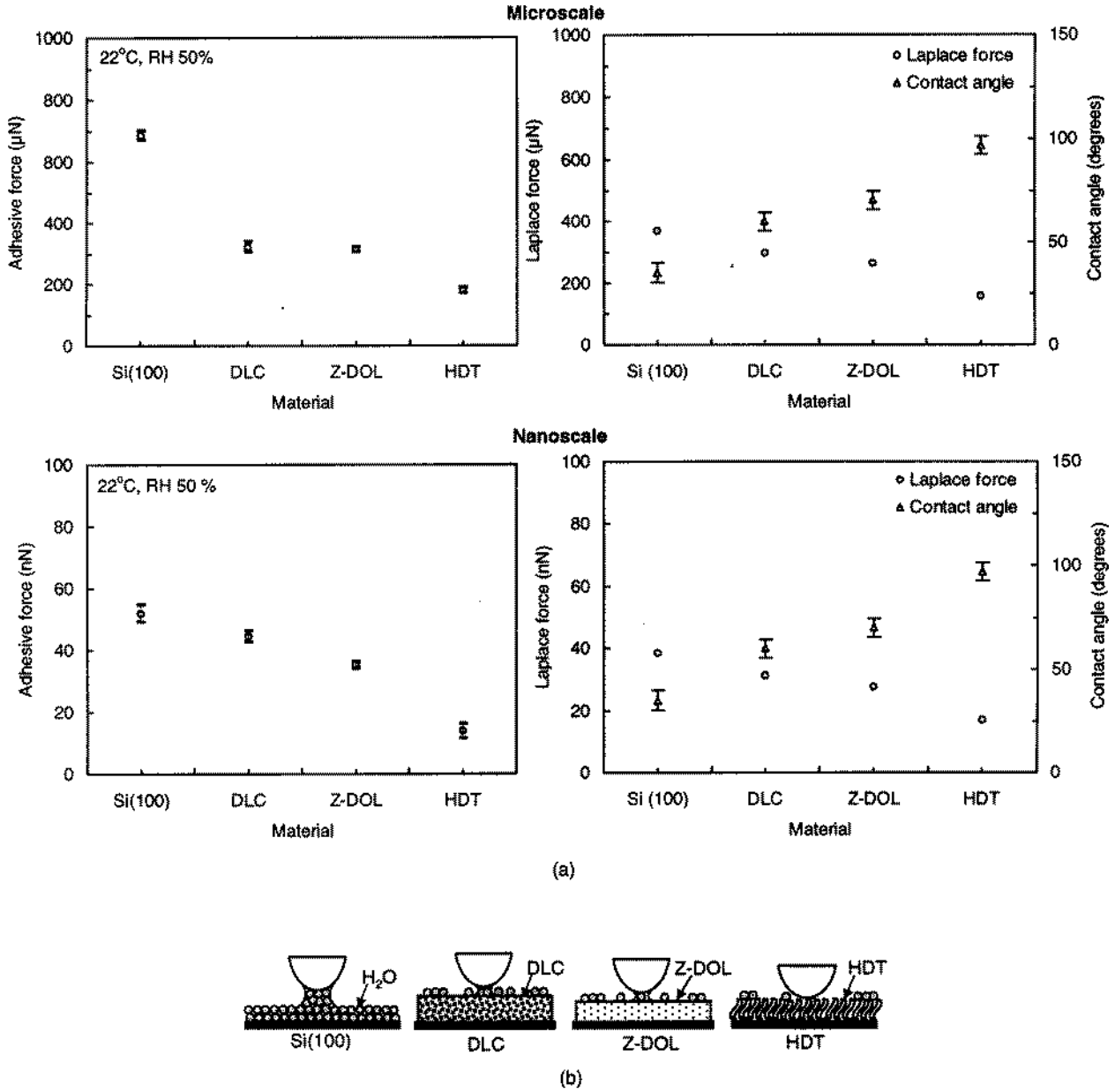

FIG. 28. (a) Adhesive forces of Si(100), DLC, chemically bonded Z-DOL, an HDT at ambient condition and the contact angle values and the calculated Laplace values, and (b) a schematic showing the relative size of water meniscus on different specimens.

and the stiction force F_s; the latter is a combination of the friction force due to the meniscus and viscous effects,[2]

$$F = F_i + F_s = \mu_r (W + F_m) + F_{v\parallel}, \tag{35}$$

where μ_r is the true coef®cient of friction in the absence of meniscus, and smaller than the measured value of $\mu = F/W$. The sum of W and F_m is the total normal load. F_m is the meniscus force in the normal direction, and $F_{v\parallel}$ is the viscous force in the sliding direction. The friction force ($\mu_r W$) depends on the material properties and surface topography, whereas F_m depends on the roughness parameters as well as the type of liquid and its ®lm thickness. $\mu_r F_m + F_{v\parallel}$ is the friction force due to liquid-mediated adhesion. In a well-lubricated contact, shearing primarily occurs in the liquid ®lm. The stress required to shear the liquid increases with an increase in the sliding velocity and the acceleration. Consequently, coef®cients of static and kinetic friction generally increase with the sliding speed or acceleration.

The coef®cient of friction, μ, including the effect of the meniscus and viscous force, is given by

$$\mu = \frac{F}{W} = \mu_r \left(1 + \frac{F_m}{W}\right) + \frac{F_{v\parallel}}{W}. \tag{36}$$

F_m and $F_{v\parallel}$ calculations can be made based on the analyses presented in the previous section. For static friction calculations at low velocities and accelerations, the viscous effect can be neglected.

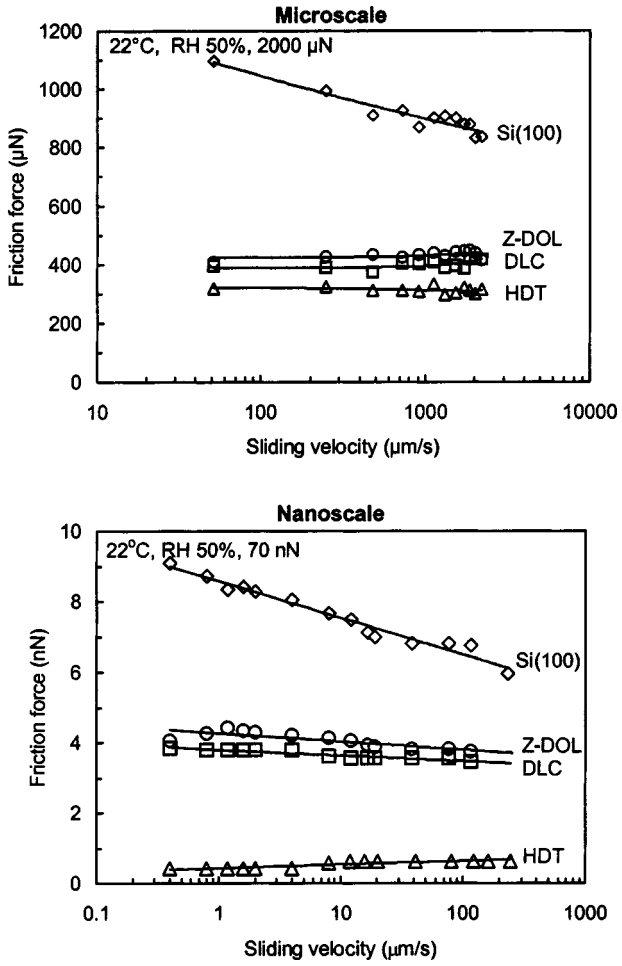

FIG. 29. In¯uence of sliding velocity on the friction forces of Si(100), DLC, chemically bonded Z-DOL, and HDT.

1. Solid ®lms

Sliding properties of DLC, chemically bonded Z-DOL, and HDT ®lms have been performed for applications to the MEMS/NEMS devices. These devices are used at a range of velocities, humidities, and temperatures. To investigate the velocity effect on friction, the friction force as a function of velocity on micro- and nanoscales was measured and is summarized in Fig. 29.[75,86] It indicates that, for Si(100), the friction force decreases logarithmically with increasing velocity. Figure 29 also indicates that the velocity has almost no effect on the friction properties of DLC, Z-DOL, and HDT. This implies that the friction mechanisms of DLC, Z-DOL, and HDT do not change with the variation of velocity. For Si(100), at high velocity, the meniscus is broken and does not have enough time to rebuild. In addition, it is also believed that tribochemical reaction plays an important role. The high velocity leads tribochemical reactions of Si(100) (which has native oxide SiO_2) with water molecules to form a $Si(OH)_4$ ®lm. This ®lm is removed and continuously replenished during sliding. The $SiOH_4$ layer at the sliding surface is known to be of low shear strength. The breaking of the water meniscus and the formation of $Si(OH)_4$ layer results in a decrease in friction force of Si(100) at higher velocity. For DLC, Z-DOL, and HDT, the surfaces exhibit hydrophobic properties, and only can adsorb few water molecules in ambient conditions. The above-mentioned meniscus breaking and tribochemical reaction mechanisms do not exist for these ®lms. Therefore, their friction force does not change with velocity.

The in¯uence of relative humidity was studied in an environmentally controlled chamber.[75,86] The adhesive force and friction force were measured by making measurements at increasing relative humidity, and the results on micro- and nanoscales are summarized in Fig. 30. It shows that for Si(100) and Z-DOL, the adhesive force increases with relative humidity, but the adhesive force of DLC shows only a very slight increase at higher humidity, while the adhesive force of HDT does not change with humidity. Figure 30 also shows that for Si(100), the friction force increases with relative humidity increase up to 45% RH, and then it shows a slight decrease with a further increase in the relative humidity. For Z-DOL, there is an increase in the friction force when humidity is higher than 45% RH. In the whole testing range, relative humidity does not have any apparent in¯uence on the friction properties of DLC and HDT. In the case of Si(100), the initial increase of relative humidity up to 45% RH causes more adsorbed water molecules, and form bigger water meniscus, which leads to an increase of friction force. But at very high humidity of 65% RH, large quantities of adsorbed water can form a continuous water layer that separates the tip and sample surfaces, and acts as a kind of lubricant, which causes a decrease in the friction force. It is observed that the humidity effect on Si(100) depends on the history of the Si(100) sample. In AFM experiments, as the surface of a Si(100) wafer readily absorbs water in air, without any pretreatment the Si(100) used in this study almost reaches its saturated stage of adsorbed water, and has in¯uence as compared to thermally treated sample (150 ÉC for 1 h) relative humidity is increased. For Z-DOL, dewetting of lubricant ®lm at humidity higher than 45% RH results in an increase in adhesive and friction forces. For DLC and HDT, the surfaces show hydrophobic properties, and increasing relative humidity does not play much of a role on their friction force.

The in¯uence of temperature was studied using a heating stage.[75,86] The adhesive force and friction force were measured in temperature range of 22±125 ÉC. The results are presented in Fig. 31. It shows that once the temperature is higher than 50 ÉC, increasing temperature causes a signi®cant decrease of adhesive and friction forces of Si(100) and a slight decrease in the case of DLC and Z-DOL. But the adhesive and friction forces of HDT do not show any apparent change with test temperature. At high temperature, desorption of water, and reduction of surface tension of water lead to decreases of adhesive and friction forces of Si(100), DLC, and Z-DOL. However, in the case of HDT ®lm, as only a few water molecules are adsorbed on the surface, the above-mentioned mechanisms do not play a big role. Therefore, the adhesive and friction forces of HDT do not show any apparent change with temperature.

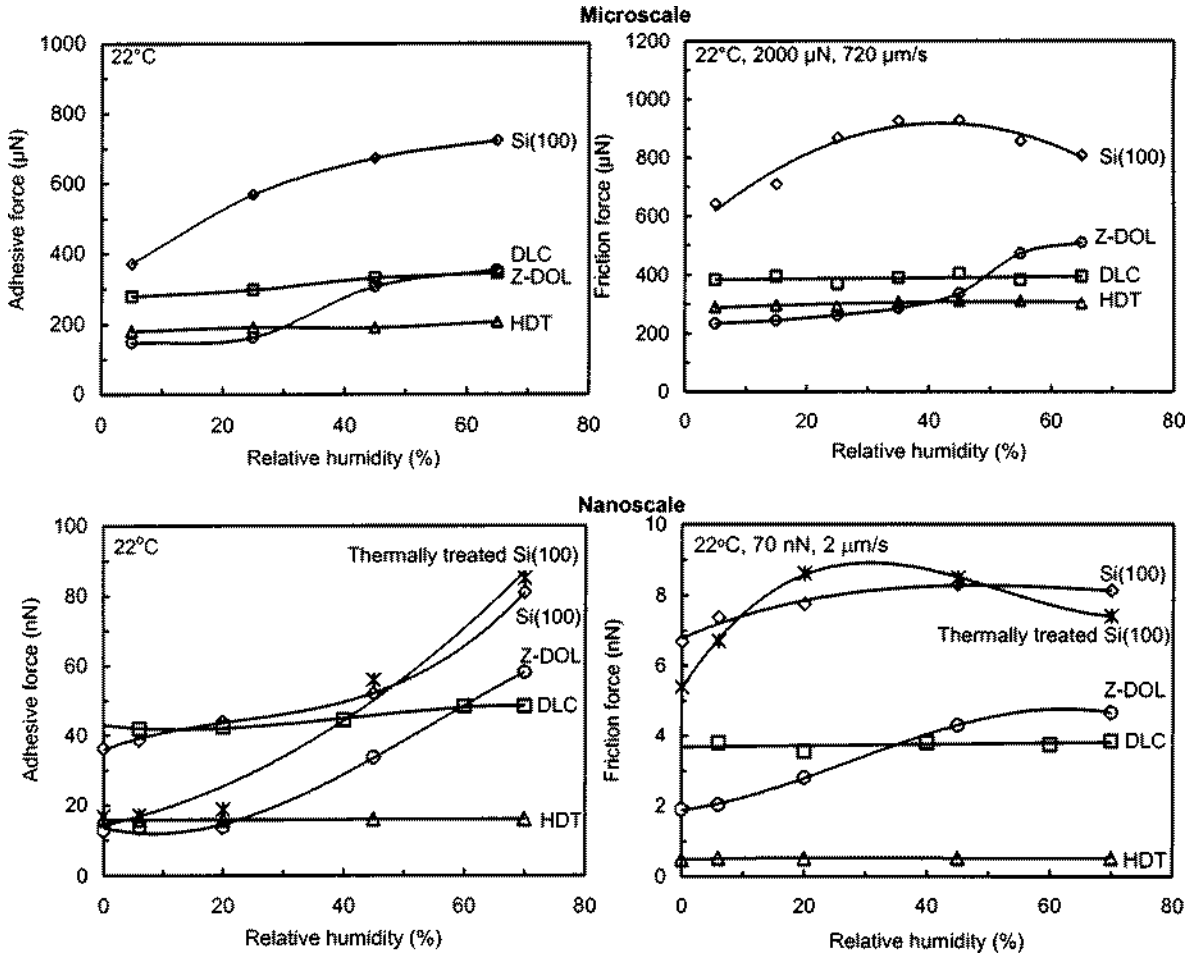

FIG. 30. In¯uence of relative humidity on the adhesive and friction forces of Si(100), DLC, chemically bonded Z-DOL, and HDT.

In summary, Figs. 29±31 show that in the entire velocity, relative humidity, and temperature test range, the adhesive force and friction force of DLC, Z-DOL, and HDT are always smaller than that of Si(100), and HDT has the smallest value.

2. Liquid ®lms

For two surfaces in contact in the presence of liquid, coef®cients of static and kinetic friction and durability are a function of the amount of liquid present at the surface with respect to the interplanar separation.[3,4] The liquid ®lm thickness and composite roughness of the interface are known to have an opposite effect on static and kinetic friction and durability; that is, an increase in ®lm thickness or a decrease in roughness results in an increase in the values of static and kinetic friction, and ®rst an increase followed by a decrease in durability (Fig. 32).[90] For rough surfaces with a composite roughness σ and a uniform liquid ®lm thickness h, to ®rst order, the static friction force, kinetic friction force, and durability are a function of h/σ[2,82,90±92] (Fig. 33). The coef®cient of friction remains low below a certain value of h/σ and increases, in some cases rapidly, beyond this value. Larger values of h/σ correspond to a larger number of asperities wetted by the liquid ®lm, resulting in larger meniscus and viscous contributions. Below the critical value, much of the liquid remains in the valleys and does not readily form menisci. It appears that for low static kinetic friction, h/σ should be less than or equal to about 0.7. Of course, if the contact is immersed in the liquid, menisci are not formed and shear occurs in the liquid ®lm, leading to very low friction. The durability data in Fig. 33 show that the durability increases with an increase in a value of h/σ. A rapid decrease in durability above a critical h/σ occurs because of a large meniscus being formed around slider edges and the presence of the stick-slip phenomenon.[90]

In a humid environment, the amount of water present at the hydrophilic interface increases with an increase in their relative humidity. The adsorbed water ®lm thickness on a diamondlike carbon-coated magnetic disk, for example, can be approximated as follows:[82]

$$h = h_1(\mathrm{RH}) + h_2 \exp[\alpha(RH-1), \tag{37}$$

where $h_1 = 0.3$ nm, $h_2 = 0.5$ nm, $\alpha = 20$, and RH is the relative humidity fraction ranging from 0 to 1. In the data shown in Fig. 34, the coef®cient of static friction of the lubricated disk increases rapidly above a relative humidity (RH) of about 60%. This critical humidity is dependent upon the interface roughness. Trends observed in Figs. 32±34 are con-

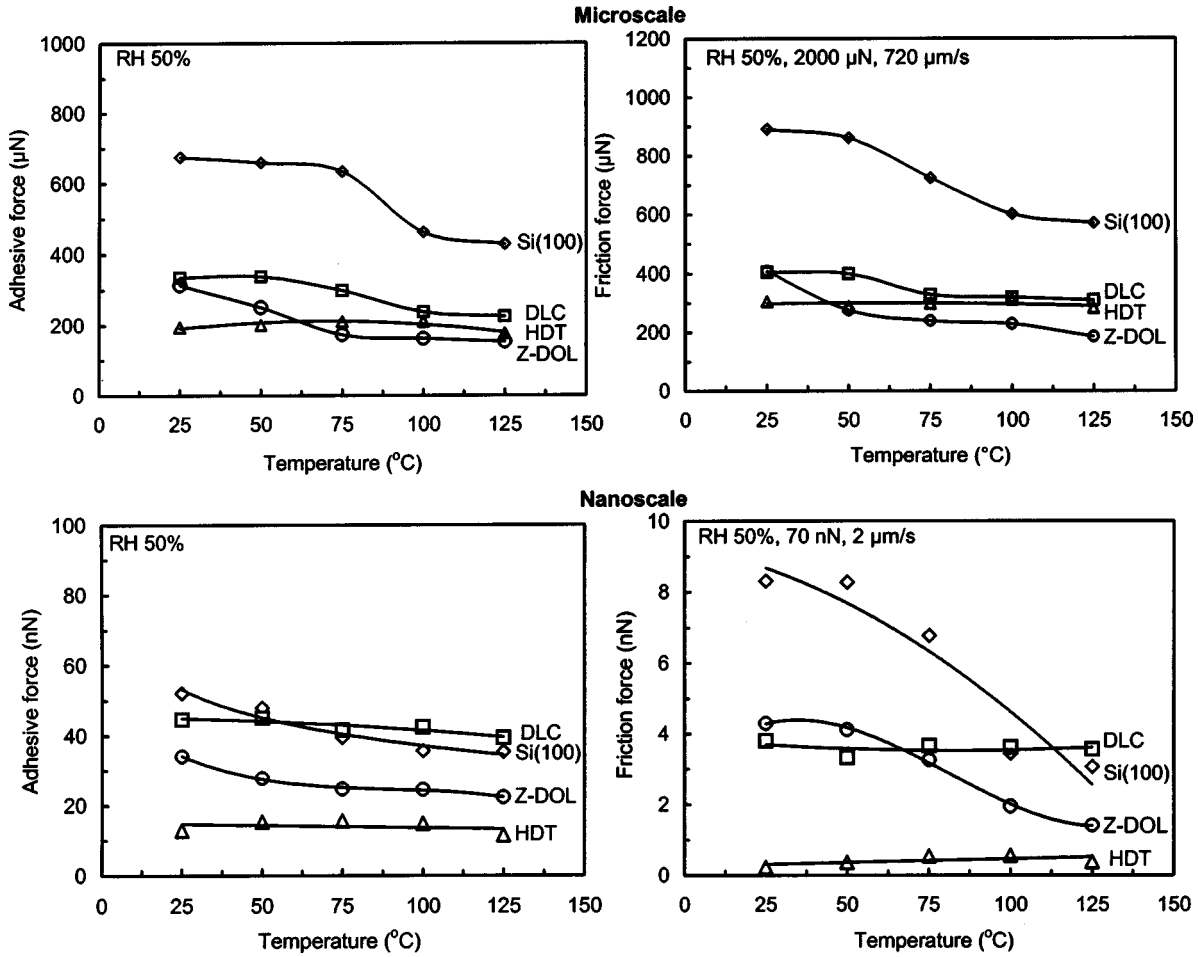

FIG. 31. Influence of temperature on the adhesive and friction forces of Si(100), DLC, chemically bonded Z-DOL, and HDT.

sistent with those predicted by contact modeling, Fig. 21. The coefficient of friction of the unlubricated disk remains low at high humidities. It is the total liquid film thickness (including water and lubricant), which contributes to the meniscus effect; therefore, an unlubricated disk can sustain much more water condensation than a lubricated disk before friction increases significantly. For kinetic friction, little change is observed. The coefficient of kinetic friction of an unlubricated disk remains unchanged with humidity, whereas the kinetic friction of a lubricated disk increases slightly above 60% RH. The durability of a lubricated disk increases with an increase in the relative humidity but decreases at high humidities. The durability of an unlubricated disk increases with an increase in humidity. Condensed water acts as lubricant and is responsible for an increase in the durability, whereas the drop in durability at high humidity in the case of a lubricated disk occurs because of high static friction.

Static friction starts to increase in some cases, rapidly beyond a certain rest time and then levels off, as shown in Fig. 35. This trend is similar to that observed for adhesive forces in Fig. 27. The rest time required for increased static friction is again dependent upon the total liquid present at the

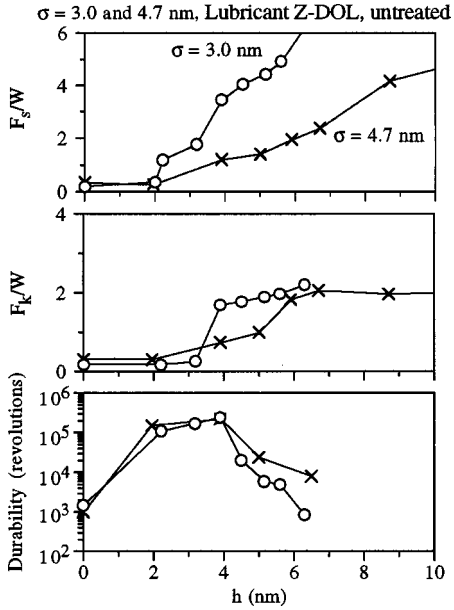

FIG. 32. Normalized static (after a rest time of 100 s) (top) and kinetic (middle) friction forces and durability in revolutions (bottom) as a function of the lubricant film thickness of lubricant Z-DOL, untreated, applied on disks with two roughnesses against a smooth slider.

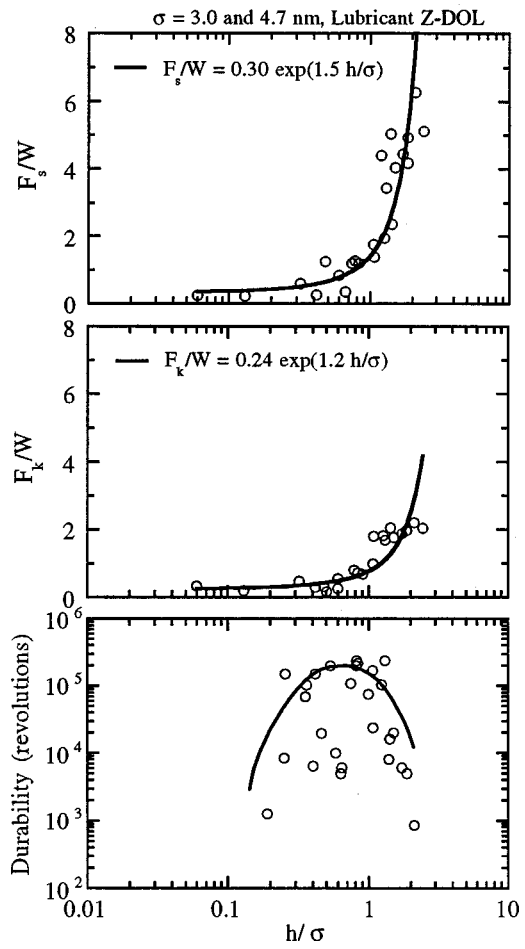

FIG. 33. Normalized static (top) and kinetic (middle) friction forces and durability in revolutions (bottom) as a function of the ratio of the lubricant ®lm thickness to composite σ roughness (h/σ). Data on untreated, partially bonded, and fully bonded Z-DOL lubricants are presented. For static and kinetic friction data, h used is a mobile fraction; for durability, h used is a total ®lm thickness.

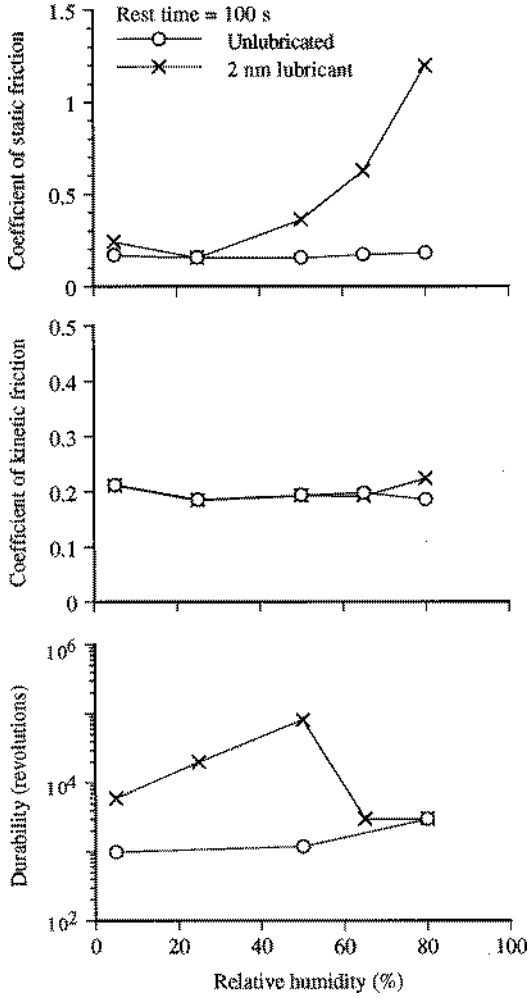

FIG. 34. Coef®cients of static friction (after a rest time of 100 s) and kinetic friction and durability as a function of relative humidity for unlubricated and lubricated disk±head interface.

interface; a lubricated disk requires less rest time than an unlubricated disk.[92]

Figure 36 shows the coef®cient of static friction as a function of acceleration.[2,91] Static friction increases with the acceleration because of viscous effects as predicted from the analysis.[3,4]

Finally, Fig. 37 shows an example of the coef®cient of friction dependence on the surface roughness for a magnetic thin-®lm rigid disk.[2] An increase in roughness results in a decrease in friction up to a certain roughness value, as expected. High roughness results in plowing.

C. Effect of tip radii and humidity on adhesion and friction

1. Experimental observations

Tip radius and relative humidity affect adhesion and friction for dry and lubricated surfaces.[74,93] Figure 38 shows the variation of single point adhesive force measurements as a function of tip radius on a Si(100) sample for several humidities. The adhesive force data are also plotted as a function of relative humidity for several tip radii. The general trend at humidities up to ambient is that a 50 nm radius Si_3N_4 tip exhibits a slightly lower adhesive force as compared to the other microtips of larger radii; in the latter case, values are similar. Thus for the microtips there is no appre-

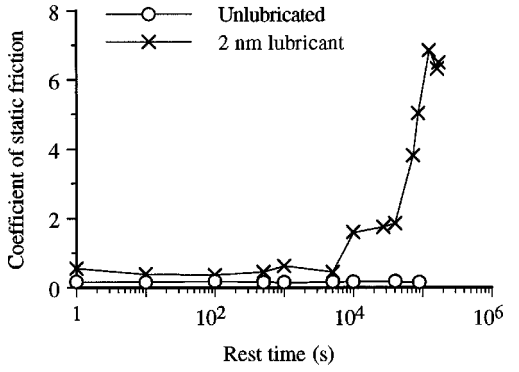

FIG. 35. Coef®cient of static friction as a function of rest time for unlubricated and lubricated disk±head interface.

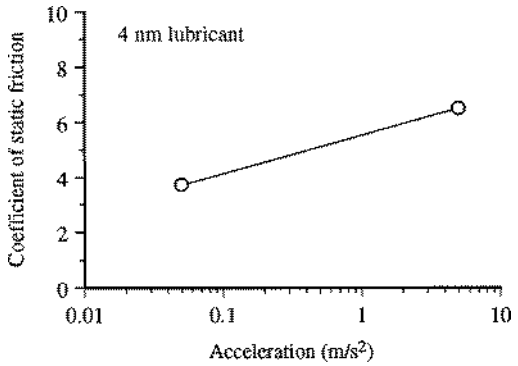

FIG. 36. Coef®cient of static friction(after a rest time of 100 s) as a function of acceleration of the disk during start-up of the magnetic disk drive.

ciable variation in adhesive force with tip radius at a given humidity up to ambient. The adhesive force increases as relative humidity increases for all tips.

Sources of adhesive force between a tip and a sample surface are van der Waals attraction and meniscus formation.[3,4] Relative magnitudes of the forces from the two sources are dependent upon various factors including the distance between the tip and the sample surface, their surface roughness, their hydrophobicity, and relative humidity.[61] For most surfaces with some roughness, the meniscus contribution dominates at moderate to high humidities. The trend in adhesive forces as a function of tip radii and relative humidity shown in Fig. 38, can be explained by the presence of meniscus forces, which arise from capillary condensation of water vapor from the environment forming meniscus bridges. If enough liquid is present to form a meniscus bridge, the meniscus force should increase with an increase in tip radius (proportional to tip radius for a spherical tip) and should be independent of the relative humidity or water ®lm thickness. In addition, an increase in tip radius in a dry environment results in increased contact area leading to higher values of van der Waals forces. However, if nanoasperities on the tip and the sample are considered then the number of contacting and near-contacting asperities forming

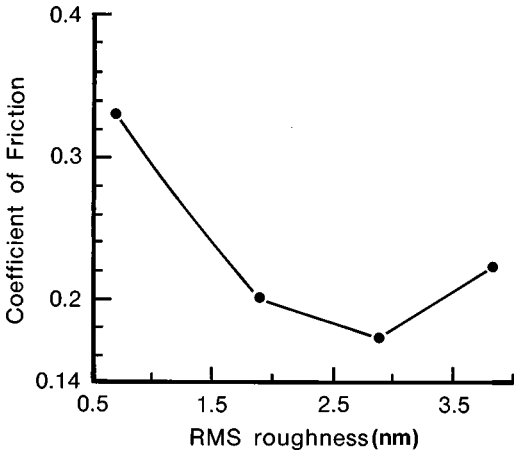

FIG. 37. Coef®cient of friction as a function of disk texture for a magnetic thin-®lm rigid disk against a ferrite slider(Ref. 2).

meniscus bridges increases with an increase of humidity leading to an increase in meniscus forces. This explains the trends observed in Fig. 38. From the data, the tip radius has little effect on the adhesive forces at low humidities but increases with tip radius at high humidity. Adhesive force also increases with an increase in humidity for all tips. This observation suggests that thickness of the liquid ®lm at low humidities is insuf®cient to form continuous meniscus bridges to affect adhesive forces in the case of all tips.

Figure 38 also shows the variation in coef®cient of friction as a function of tip radius at a given humidity, and as a function of relative humidity for a given tip radius for Si(100). It can be observed that for 0% RH, the coef®cient of friction is about the same for the tip radii except for the largest tip, which shows a higher value. At all other humidities, the trend consistently shows that the coef®cient of friction increases with tip radius. An increase in friction with tip radius at low to moderate humidities arises from increased contact area (higher van der Waals forces) and higher values of shear forces required for larger contact area. At high humidities, similar to adhesive force data, an increase with tip radius occurs because of both contact area and meniscus effects. Although AFM/FFM measurements are able to measure the combined effect of the contribution of van der Waals and meniscus forces toward friction force or adhesive force, it is dif®cult to measure their individual contributions separately. It can be seen that for all tips, the coef®cient of friction increases with humidity to about ambient, beyond which it starts to decrease. The initial increase in the coef®cient of friction with humidity arises from the fact that the thickness of the water ®lm increases with an increase in the humidity, which results in a larger number of nanoasperities forming meniscus bridges and leads to higher friction (larger shear force). The same trend is expected with the microtips beyond 65% RH. This is attributed to the fact that at higher humidities, the adsorbed water ®lm on the surface acts as a lubricant between the two surfaces. Thus the interface is changed at higher humidities, resulting in lower shear strength and hence lower friction force and coef®cient of friction.

2. Adhesion and friction force expressions for a single asperity contact

We now obtain the expressions for the adhesive force and coef®cient of friction for a single asperity contact with a meniscus formed at the interface. For a spherical asperity of radius R in contact with a ¯at and smooth surface with the composite modulus of elasticity E^* and with a concave meniscus, the attractive meniscus force (adhesive force) F_m or W_{ad} is given by Eq. (12a). For an elastic contact for both extrinsic (W) and intrinsic (W_{ad}) normal load, the friction force is given as

$$F_e = \pi\tau\left[\frac{3(W+W_{ad})R}{4E^*}\right]^{2/3}, \tag{38}$$

where τ is the average shear strength of the contacts (surface energy effects are not considered here). Note that adhesive force increases linearly with an increase in the tip radius, and

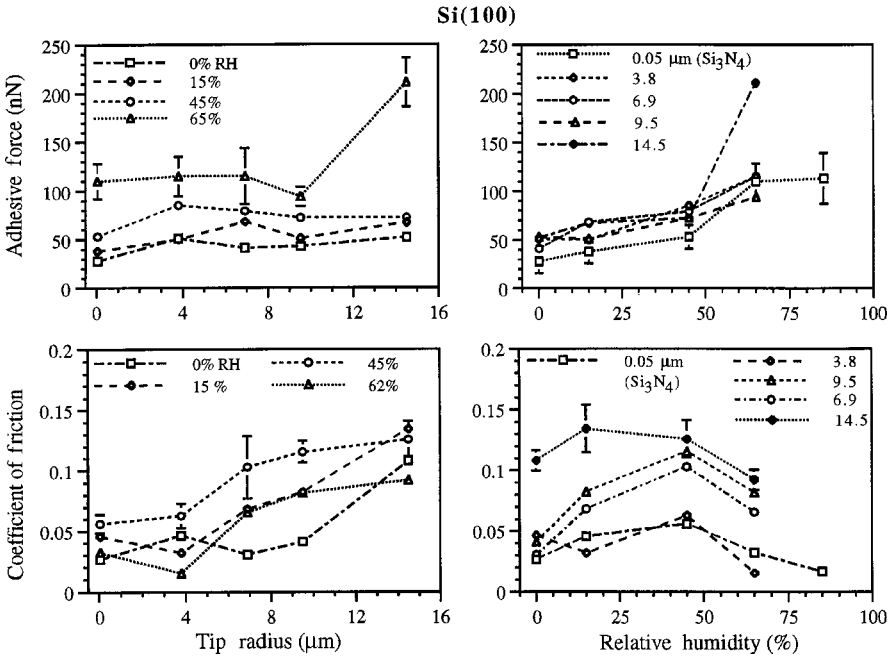

FIG. 38. Adhesive force and coef®cient of friction as a function of tip radius at several humidities and as a function of relative humidity at several tip radii on Si(100)ÐRef. 93.

the friction force increases with an increase in tip radius as $R^{2/3}$ and with normal load as $(W+W_{ad})^{2/3}$. The experimental data in support of $W^{2/3}$ dependence on the friction force can be found in various references.[94] The coef®cient of friction μ_e is obtained from Eq. (38) as

$$\mu_e=\frac{F_e}{(W+W_{ad})}=\pi\tau\left[\frac{3R}{4E^*}\right]^{2/3}\frac{1}{(W+W_{ad})^{1/3}}. \tag{39}$$

In the plastic contact regime,[3,4] the coef®cient of friction μ_p is obtained as

$$\mu_p=\frac{F_p}{(W+W_{ad})}=\frac{\tau}{H_s}, \tag{40}$$

where H_s is the hardness of the softer material. Note that in the plastic contact regime, the coef®cient of friction is independent of external load, adhesive contributions, and surface geometry.

For comparison, for multiple asperity contacts in the elastic contact regime the total adhesive force W_{ad} is the summation of adhesive forces at n individual contacts,[3,4]

$$W_{ad}=\sum_{i=1}^{n}(W_{ad})_i \tag{41}$$

and

$$\mu_e\approx\frac{3.2\tau}{E^*(\sigma_p/R_p)^{1/2}+(W_{ad}/W)},$$

where σ_p and R_p are the standard deviation of summit heights and average summit radius, respectively. Note that the coef®cient of friction depends upon the surface roughness. In the plastic contact regime, the expression for μ_p in Eq. (40) does not change with surface roughness.

The source of the adhesive force, in a wet contact in the AFM experiments being performed in an ambient environment, includes mainly attractive meniscus force due to capillary condensation of water vapor from the environment. The meniscus force for a single contact increases with an increase in tip radius. A sharp AFM tip in contact with a smooth surface at low loads (on the order of a few nN) for most materials can be simulated as a single-asperity contact. At higher loads, for rough surfaces and for soft surfaces, multiple contacts would occur. Furthermore, at low loads (nN range) for most materials, the local deformation would be primarily elastic. Assuming that shear strength of contacts does not change, the adhesive force for smooth and hard surfaces at low normal load (on the order of few nN) (for a single asperity contact in the elastic contact regime) would increase with an increase in tip radius, and the coef®cient of friction would decrease with an increase in total normal load as $(W+W_{ad})^{-1/3}$ and would increase with an increase of tip radius as $R^{2/3}$. In this case, the Amontons law of friction, which states that coef®cient of friction is independent of normal load and is independent of apparent area of contact, does not hold. For a single-asperity plastic contact and multiple-asperity plastic contacts, neither the normal load nor the tip radius come into play in calculation of coef®cient of friction. In the case of multiple-asperity contacts, the number of contacts increases with an increase of normal load, therefore adhesive force increases with an increase in load.

In the data presented earlier in this section, the effect of tip radius and humidity on the adhesive forces and coef®cient of friction is investigated for experiments with a Si(100) surface at loads in the range of 10±100 nN. The multiple asperity elastic-contact regime is relevant for this study. An increase in humidity generally results in an increase in the number of meniscus bridges, which would increase the adhesive force. As suggested earlier, that increase in humidity also may decrease shear strength of contacts. A combination of an increase in adhesive force and a decrease

TABLE I. Typical adhesive force and friction force data on micro- and nanoscales of various samples in air.

Sample	Adhesive force		Coef®cient of friction (μ)	
	Microscale[a] (μN)	Nanoscale[b] (nN)	Microscale[a]	Nanoscale[b]
Si(100)	685	52	0.47	0.07
DLC	325	44	0.19	0.03
Z-DOL	315	35	0.23	0.04
HDT	180	14	0.15	0.006

[a]Versus 500 mm radius Si(100) ball.
[b]Versus 50 nm radius Si_3N_4 tip.

in shear strength would affect the coef®cient of friction. An increase in tip radius would increase the meniscus force (adhesive force). A substantial increase in the tip radius may also increase interatomic forces. These effects in¯uence the coef®cient of friction with an increase in the tip radius.

D. Scale dependence on friction

Table I summarizes adhesive force and friction data. Adhesive force and coef®cient of friction values on nanoscale are much lower than that at microscale.[86] Scale dependence is clearly observed in these data. As further evidence of scale dependence, Table II shows the coef®cient of friction measured for single-crystal graphite, SiO_2, and natural diamond on nano- and macroscales.[95] It is clearly observed that friction values are scale dependent. The values on the nanoscale are much lower than those on the micro- and macroscale.

There are at least the following four (and possibly more) differences in the operating conditions responsible for the differences in friction values. First, the contact stresses at AFM conditions, in spite of small tip radii, generally do not exceed the sample hardness; that minimizes plastic deformation. Average contact stresses in micro/macrocontacts are generally lower than that in AFM contact. However, a large number of asperities come into contact and some go through some plastic deformation. Second, when measured for the small contact areas and very low loads used in nanoscale studies, indentation hardness is higher than at the macroscale.[3,4,96] Lack of plastic deformation and improved mechanical properties reduce the degree of friction and wear. Third, the small apparent area of contact reduces the number of particles trapped at the interface, and thus minimizes the third-body plowing contribution to the friction force.[4] As a fourth and ®nal difference, we have seen in the previous section that coef®cient of friction increases with an increase in the AFM tip radius. AFM data are taken with a sharp tip, whereas the size of asperities in contact in macro/microscale tests range from nanoasperities to much larger asperities which may be responsible for larger values of friction force on macro/microscale.

Scale effects in friction have recently been modeled by Bhushan and Nosonovsky.[97] According to this model, scale effects play a big role in friction.

TABLE II. Surface roughness (standard deviation of surface heights of σ) and coef®cients of friction on nano-/micro- and macroscales of various samples in air.

Material	σ (nm)	Coef®cient of nanoscale friction versus Si_3N_4 tip[a]	Coef®cient of macroscale friction versus Si_3N_4 ball[b]
Graphite (HOPG)	0.09	0.006	0.1
Natural diamond	2.3	0.04	0.2
Si(100)	0.14	0.07	0.4

[a]Tip radius of about 50 nm in the load range of 10±150 nN (2.5±6.1 GPa) and a scanning speed of 0.5 nm/s and scan area of 1 nm×1 nm for HOPG and a scanning speed of 4 μm/s and scan area of 1 μm×1 μm for diamond and Si(100).
[b]Ball radius of 3 mm at a normal load of 1 N (0.6 GPa) and average sliding speed of 0.8 mm/s.

V. EXAMPLES OF METHODS TO REDUCE ADHESION AND STICTION IN MAGNETIC STORAGE AND MEMS/NEMS APPLICATIONS

A variety of techniques have been proposed, and some are used in commercial applications, to reduce stiction. If the source of high adhesion and static friction (stiction) is liquid mediated adhesion, then surface energy, the amount of mobile liquid present at the interface, and/or contact area need to be minimized. Surface energy can be reduced by providing a hydrophobic surface. The amount of mobile liquid can be reduced by using solid lubricants or partially chemically bonded liquid ®lms or by controlling relative humidity. The contact area can be reduced by introducing roughness or bumps on the surfaces and/or by having stiffer/harder surfaces, or by reducing the apparent size of one of the bodies. Stiction reduction is especially important in devices with smooth surfaces which involve relative motion under light loads. In these devices, in the presence of liquid ®lm, meniscus forces may be large and in some cases much larger than the external load. In close proximity (0.5±5 nm), van der Waals forces may also be signi®cant. Examples of devices in which stiction is important include magnetic storage devices and MEMS/NEMS devices which involve relative motion. Some details follow.

A. Magnetic storage devices

Magnetic storage devices are used for data storage. These include rigid disk drives, tape drives, and ¯exible disk drives.[2] Under steady operating conditions, a hydrodynamic air ®lm is developed at the head-medium interface. However, a continuous physical contact occurs during start±stop operations of the drives. Stiction, friction, and wear limit their reliability, stiction being a more important issue! Sources of liquid present at the interface responsible for liquid mediated adhesion or stiction are capillary condensation of the water vapor from the environment and deliberately applied liquid ®lms for durability. Stiction is minimized by optimization of the surface roughness, interface geometry, and interface materials, including lubricant ®lms.

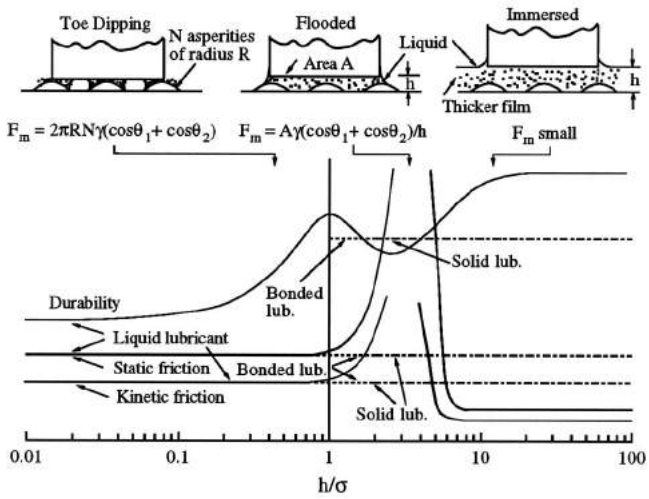

FIG. 39. Schematic showing the effect of h/σ on static, kinetic friction, and durability and associated mechanisms for a lubricated interface.

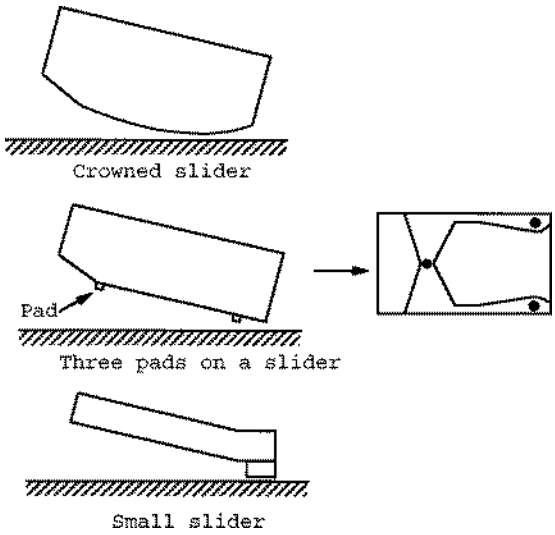

FIG. 40. Schematic showing various types of geometrical design (size and shape) of a slider for low stiction in near-contact recording applications.

1. Lubrication methods and slider designs in rigid disk drives

The effect of liquid ®lm thickness(h) and interface roughness (σ) on static and kinetic friction forces and durability is summarized in Fig. 39.[82] Film thickness h is the total thickness of the mobile fraction of the liquid ®lm, which includes the lubricant ®lm plus the water ®lm(condensation of water vapor from the environment) on disk and head slider surfaces for static and kinetic friction, but h is the total thickness of the liquid ®lm for durability; and σ is the composite roughness of disk and head slider surfaces. The vertical axis indicates the normalized static friction (F_s/W), normalized kinetic friction (F_k/W), and durability in terms of disk revolutions or contact±start±stop (CSS) cycles. Note that a high h/σ (10), which is in the immersed region, is desirable for low static and kinetic friction and long durability. At the intermediate value of h/σ (between ~0.7 and 6), stiction increases with an increase of h/σ in the range of about 0.7±2 for the head/disk interface and remains high up to the ratio of about 6. Durability is poor at low h/σ, and gradually increases with h/σ up to about 1. It slightly decreases with increasing h/σ and then increases and approaches a high value at $h/\sigma > 10$. In general, smooth surfaces and surfaces with thick ®lms result in low wear. Bonded and solid lubricants can be used to maintain low stiction, friction, and wear. Reduction in the slider size and load can also be used to reduce the stiction.

Thick ®lms have been known to be undesirable because of slider instability during accessing and contamination resulting from recirculation of the lubricant required for thick ®lms. Therefore, partially bonded thin-®lm lubrication with h/σ (mobile fraction ®lm/composite σ roughness between 0.5 and 0.7) is recommended. Further optimization can be obtained with a smooth surface, small slider size, and low load. In a ¯ooded interface, the apparent contact area needs to be reduced to reduce stiction. The apparent contact area between the disk and head slider surfaces can be reduced by either providing a crown on the slider, using three pads on the slider surface, or reducing the physical size of the slider (Fig. 40).[82] Wear of the interface can be high if the apparent contact area is signi®cantly reduced; thus, the slider shape and size need to be optimized.

2. Roughness distributions in rigid disks

Surface roughness of rigid disk surfaces is optimized in the landing zone to minimize stiction and friction. Historically, the disks are polished to a desired roughness using either free or ®xed abrasives.[98] During the past decade, a laser texturing process is used to provide ``patterned surfaces" with precise and controllable topography. In the laser texturing process, a high-energy, pulsed laser is used to rapidly melt a microscopic area of a disk substrate, the surface tension causes the pool to deform, and the molten pool is instantaneously solidi®ed.[84] This creates discrete topographic features. The features used in the disk industry are either rounded, dome-like protrusions (sombrero shaped) or craters (V or W type or donut shaped), usually known as bumps; see Fig. 41. Typical sombrero, V and W type bumps have about 10 to 15 μm rim diameters and heights of about 15±25 nm with about a 50 μm×50 μm pitch. This gives on the order of 400 000 bumps in the landing zone of a 95-mm-diam disk.

The stiction phenomena at the head/disk interface can be controlled by controlling the size, shape, and number of the laser bumps. Studies to identify an optimum bump shape and the relationship between the optimum number of bumps as a function of the bump geometry for various bump shapes have been conducted by Bhushan and co-workers.[84,99] The following design methodology has been used to determine an optimum number of bumps. For a given size and shape, the meniscus force increases with an increase in the number of bumps. Thus, it is important to minimize the number of bumps to control the stiction phenomenon. On the other hand, too few bumps can result in the failure of a disk surface due to plastic deformation and wear. To prevent the

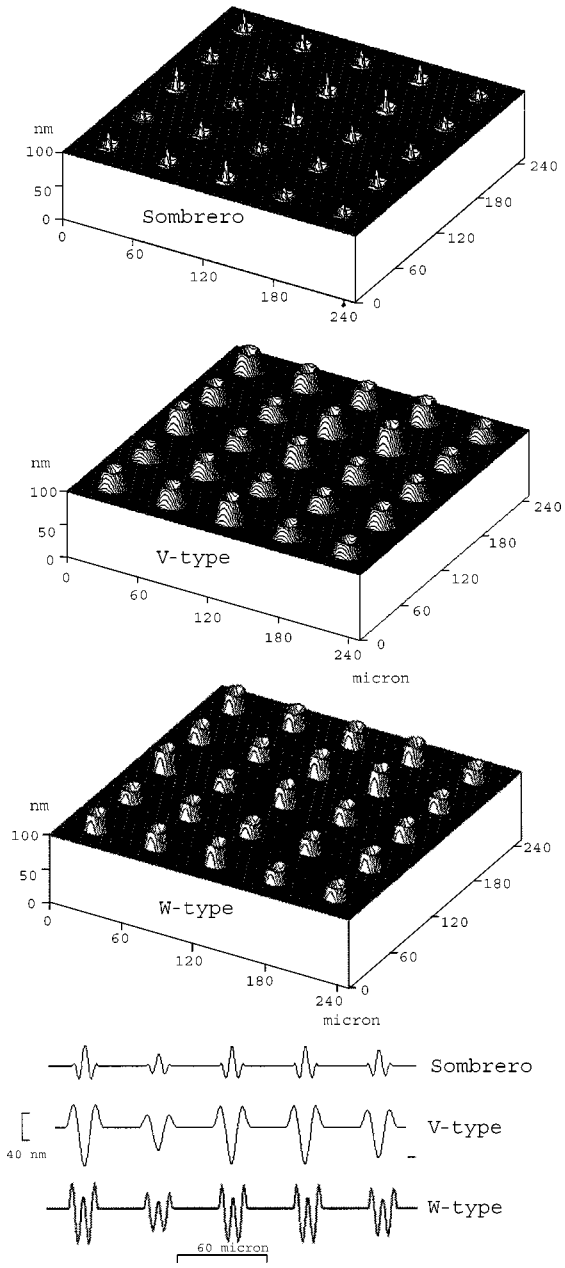

FIG. 41. Three-dimensional surface plots (top) and two-dimensional line plots (bottom) of sombrero, V, and W type laser surfaces ($R_{rim}=7.5\ \mu$m, $H_{mean}=25$ nm, $\sigma=5$ nm) with a Gaussian height distribution.

bumps from yielding, the number of bumps on the disk surface should be greater than a certain minimum, which would also give a lower bound for the stiction. Numerical analyses of computer-generated surfaces are used to predict an optimum number of bumps.

3. Some approaches in tape drives

The friction between the tape and bearing surfaces (magnetic head and other support bearings in the tape path) can be reduced by suitable acoustic excitation of the tape or the bearing surface. High-frequency (a few Hz to few kHz) oscillation of a surface with a small amplitude (a few microns) produces an intermittent separation of the bearing surface

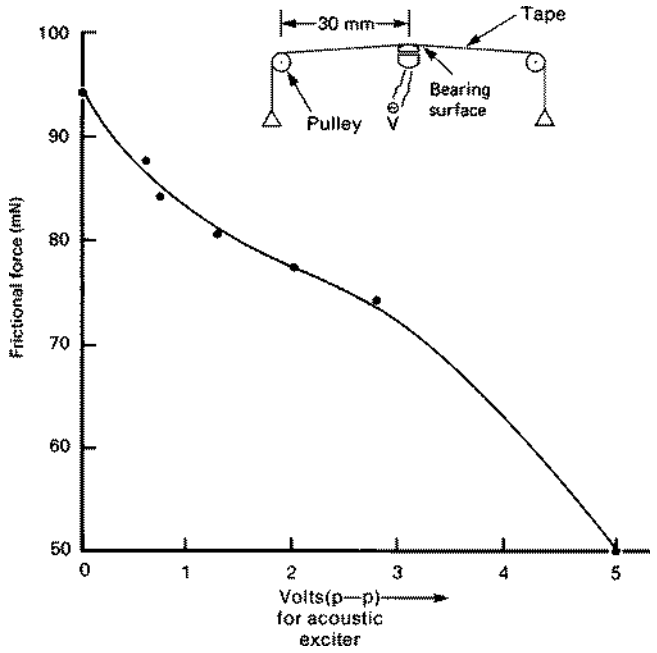

FIG. 42. Effect of acoustic excitation on friction for a magnetic tape (Ref. 100).

from the tape at ®rst. This sucks in air, producing a thin air ®lm between the tape and the bearing surface. This is known as the squeeze-®lm effect.[3,4] Tam and Bhushan[100] stretched a magnetic tape onto contact with a spherical glass surface that was acoustically excited by a small coil (loud speaker). The coil was connected to a signal generator that provided an oscillating voltage of amplitudes less than 5 V (peak-to-peak) at frequencies in the range of 10 ± 10^4 Hz. The friction as a function of the oscillating voltage is shown in Fig. 42 for an acoustic excitation frequency in the range of 100 ± 1000 Hz. Note that the reduction of friction by at least a factor of 2 was achieved. Frequencies used in the measurements were in the audio range, but any suitable frequency, such as subsonic or ultrasonic frequencies, may also be possible.

Tam and Bhushan[100] proposed two examples of possible embodiment of acoustic excitation in a tape-bearing interface (Fig. 43). In the concepts shown in the ®gure, the bearing surface is vibrated by a radio frequency (oscillating) electrical pulse in the range of audio to video frequencies applied to a piezoelectric element attached to the bearing surface. For a head-tape interface application, friction reduction is only necessary during the start/stop duration, and a rf pulse of duration long enough to last the start or stop duration is selected. For applications to the bearing in the tape path other than the magnetic head, a rf pulse can be continuously applied.

B. MEMS/NEMS

In a number of MEMS/NEMS devices involving relative motion, stiction may limit the lifetime and compromise the performance and reliability.[19] A variety of MEMS devices have been produced and some are used commercially. MEMS for mechanical applications include acceleration,

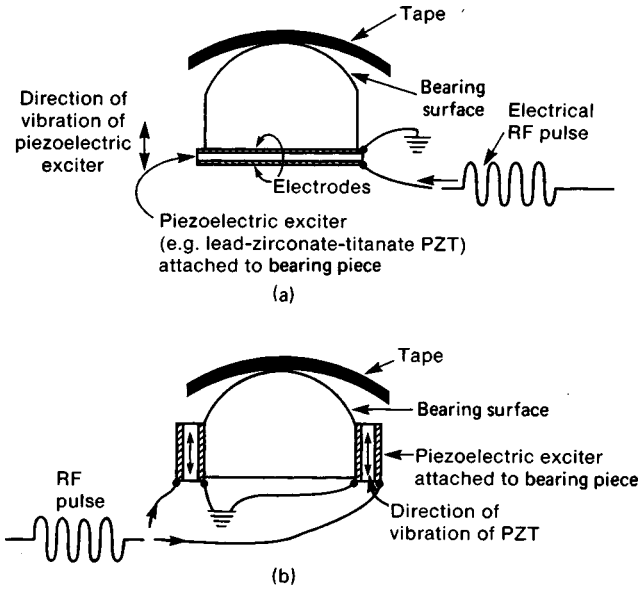

FIG. 43. Examples of possible embodiment of acoustic excitation for a tape-bearing interface: (a) an end-on excitation con®guration, and (b) side-on excitation con®guration (Ref. 100).

pressure, ¯ow, and gas sensors, linear and rotary actuators, and other microstructures or microcomponents such as electric motors, gear trains, gas turbine engines, nozzles, ¯uid pumps, ¯uid valves, and switches. Two major MEMS devices involving relative motion are integrated capacitive-type silicon accelerometers used for deployment of air bags in automobiles and for the consumer electronics market[101,102] and digital micromirror devices (DMD) for digital projection displays in portable and home theater projectors as well as table top and projection TVs.[103±105] In an accelerometer, shown in Fig. 44, the central suspended beam mass (about 0.7 μg) is supported on the four corners by spring structures. The central beam has interdigitated cantilevered electrode ®ngers (about 125 μm long and 3 μm thick) on all four sides that alternate with those of the stationary electrode ®ngers as shown, with about 1.3 μm gaps. Lateral motion of the central beam causes a change in the capacitance between these electrodes, which is used to measure the acceleration. Here stiction between the adjacent electrodes as well as stiction of the beam structure with the underlying substrate are detrimental to the operation of the sensor.[101,102] Wear during unintended contacts of these polysilicon ®ngers is also a problem. A subnanometer thick phenylsiloxane lubricant ®lm is used on the electrodes to reduce stiction and wear.

Figure 44 also shows two DMD pixels. The surface micromachined array (chip set) consists of half a million to more than two million of these independently controlled re¯ective, micromirrors (mirror size on the order of 14 μm square and 15 μm pitch) which ¯ip backward and forward at a frequency on the order of 5000 times a second. For the binary operation, micromirror/yoke structure mounted on torsional hinges is rotated at ± 10É (with respect to the horizontal plane) as a result of electrostatic attraction between the micromirror structure and the underlying memory cell, and is limited by a mechanical stop. Contact between cantilevered spring tips at the end of the yoke (four present on each yoke) with the underlying stationary landing sites is required for true digital (binary) operation. Stiction and wear during a contact between aluminum alloy spring tips and

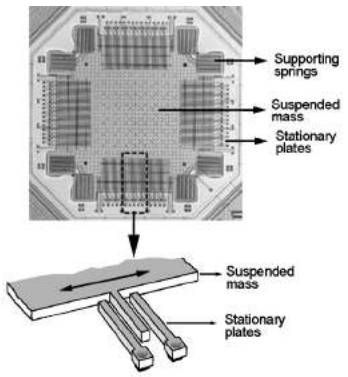

Capacitive type silicon accelerometer for automotive sensory applications (Sulouff, 1998)

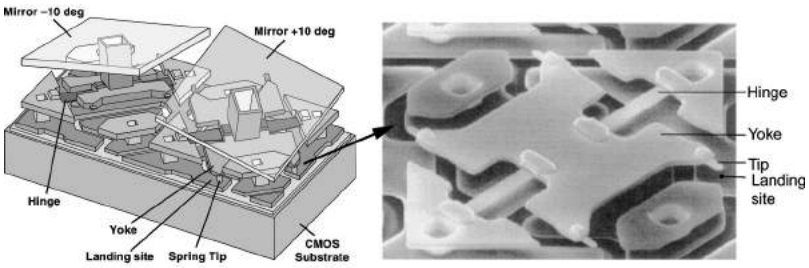

Digital micromirror device for displays (Hornbeck, 1999)

FIG. 44. (a) Integrated capacitive-type silicon accelerometer, and (b) two digital micromirror device (DMD) pixels used in digital light processing (DLP) technology for digital projection displays.

TABLE III. Surface roughness parameters and coef®cient of microscale friction for various micromotor component surfaces measured using an AFM. Mean and $\pm 1\sigma$ values are given.

	rms roughness[a] (nm)	Peak-to-valley distance[a] (nm)	Skewness,[a] Sk	Kurtosis,[a] K	Coef®cient of microscale friction[b] (μ)
Rotor topside	21±0.6	225±23	1.4±0.30	6.1±1.7	0.07±0.02
Rotor underside	14±2.4	80±11	−1.0±0.22	3.5±0.50	0.11±0.03
Stator topside	19±1	246±21	1.4±0.50	6.6±1.5	0.08±0.01

[a]Measured from a tapping mode AFM scan of size 5 μm×5 μm using a standard Si tip scanning at 5 μm/s in a direction orthogonal to the long axis of the cantilever.
[b]Measured using an AFM in contact mode at 5 μm×5 μm scan size using a standard Si_3N_4 tip scanning at 10 μm/s in a direction parallel to the long axis of the cantilever.

landing sites and sensitivity to particles in the chip package and operating environment are some of the important issues affecting the reliable operation of a micromirror device. Per¯uorodecanoic acid (PFDA) self-assembled monolayers, applied by a vapor deposition process are used on the tip and landing sites to reduce stiction and wear.[106] The spring tip is used in order to use the spring stored energy to pop up the tip during pull-off. A lifetime estimate of over one hundred thousand operating hours with no degradation in image quality is the norm.

There are also a number of NEMS/BioNEMS devices where adhesion, friction, and wear issues are important.[19] For example, in intravascular micro/nanoscale drug delivery devices used for search and destroy disease cells, these microdevices are injected into the blood stream, and they travel freely through the circulatory system.[24,25,107] In order to direct these drug-delivery particles to cancer sites, their external surfaces are chemically modi®ed to carry molecules that have lock-and-key binding speci®city with molecules that support a growing cancer mass. As soon as the particles dock to the cells, a compound is released that forms a pore on the membrane of the cells which leads to cell death and ultimately to the cancer mass that was nourished by the blood vessel. Adhesion between particles and cancer cells is key to successful operation of these drug delivery devices.

1. Roughness studies

Surface roughness of the surfaces usually has a strong in¯uence on the friction characteristics on the micro/nanoscale. Roughness measurements on various microfabricated component surfaces of a micromotor were made by Sundararajan and Bhushan.[89] Table III shows various surface roughness parameters obtained from 5 μm×5 μm scans of the various component surfaces of several micromotors using the AFM in tapping mode. A surface with a Gaussian height distribution has a skewness of zero and kurtosis of three. Although the rotor and stator top surfaces exhibit comparable roughness parameters, the underside of the rotors exhibits lower rms roughness and peak-to-valley distance values. More importantly, the rotor underside shows negative skewness and lower kurtosis than the topsides, both of which are conductive to high real area of contact and hence high friction.[3,4,72] The rotor underside also exhibits higher coef®cient of microscale friction than the rotor topside and stator, as shown in Table III.

Figure 45 shows representative surface height maps of the various surfaces of a micromotor measured using the AFM in tapping mode. The rotor underside exhibits varying topography from the outer edge to the middle and inner edge. At the outer edges, the topography shows smaller circular asperities, similar to the topside. The middle and inner regions show deep pits with ®ne edges that may have been created by the etchants used for etching of the sacri®cial layer. It is known that etching can affect the roughness of surfaces in surface micromachining. The residence time of the etchant near the inner region is high, which is responsible for larger pits. The fabrication process should be optimized to realize near optimum surface roughness of the contacting surfaces.

The analysis of separation distance dependence on meniscus and van der Waals forces presented earlier (Fig. 23) can be used in the design of surface roughness in MEMS/NEMS. For example in DMDs, if the tip is in close proximity (on the order of 0.5 nm), van der Waals forces may be dominant over meniscus forces. van der Waals forces can be minimized by increasing the surface roughness. Increased surface roughness also reduces the meniscus forces.

2. Lubrication studies

The viability of chemically bonded per¯ourorpolyether lubricant ®lms of Z-DOL for micromotors was investigated and the effect of humidity on the friction forces of unlubricated and lubricated devices was studied by Sundararajan and Bhushan.[89] Figure 46 summarizes static friction force data for two motors, M1 and M2, along with schematics of the meniscus effects for the unlubricated and lubricated surfaces. Static friction force was measured by pushing a rotor using an AFM tip and measuring the lateral force required to initiate its relative motion.[89] For unlubricated surfaces, menisci are formed at moderate to high humidity, resulting in high friction force between the surfaces. The formation of meniscus bridges is supported by the fact that the static friction force for unlubricated motors increased at high humidity as reported by Sundararajan and Bhushan.[89] Solid bridging may occur near the rotor±hub interface due to silica residues

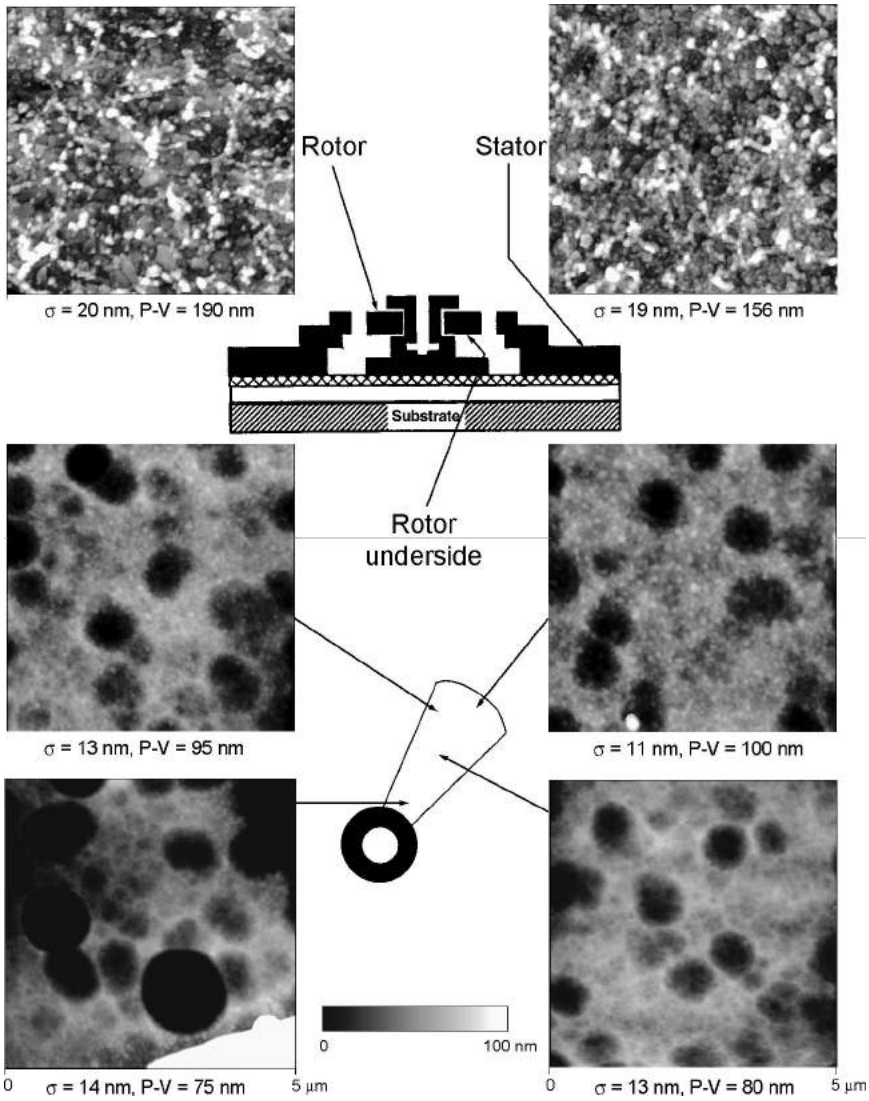

FIG. 45. Representative AFM surface height images obtained in tapping mode (5 μm×5 μm scan size) of various component surfaces of a micromotor. RMS roughness and peak-to-valley values of the surfaces are given. The underside of the rotor exhibits drastically different topography from the topside (Ref. 89).

after the ®rst etching process. In addition the drying process after the ®nal etch can result in liquid bridging formed by the drying liquid due to meniscus force at these areas.[17,19,77] The initial static friction force therefore will be quite high. Once the ®rst movement of the rotor permanently breaks these solid and liquid bridges, the static friction force of the motors will drop to a value dictated predominantly by the adhesive energies of rotor and hub surfaces, the real area of contact between these surfaces and meniscus forces due to water vapor in the air. Figure 46 shows that lubrication with a mobile layer, even a thin one, results in very high static friction forces due to meniscus effects of the lubricant liquid itself at and near the contact regions. It should be noted that a motor submerged in a liquid lubricant would result in a fully ¯ooded lubrication regime. In this case there is no meniscus contribution and only the viscous contribution to the friction forces would be relevant. However, submerging the device in a lubricant may not be a practical method. A solid-like hydrophobic lubricant layer (such as bonded Z-DOL) results in favorable friction characteristics of the motor, as shown in Fig. 46. The hydrophobic nature of the lubricant inhibits meniscus formation between contact surfaces and maintains low friction even at high humidity. This suggests that solid-like hydrophobic lubricants are good for lubrication of MEMS while the use of mobile lubricants result in increased values of static friction force.

3. Issues in fabrication processes

There are tribological issues in the fabrication processes as well. For example, the last step in the surface micromachining involves the removal of sacri®cial layer(s), called release, since the microstructures are released from the surrounding sacri®cial layer(s). The release is accomplished by an aqueous chemical etch, rinsing and drying processes. Due to meniscus effects as a result of wet processes, the suspended structures can sometimes collapse and permanently adhere to the underlying substrate, as shown in Fig. 47. Several methods have been proposed to avoid this, so-called, release stiction.[16] These include CO_2 critical point drying at high pressure,[108] the use of temporary support structures to counteract the surface tension forces,[109] introduction of anti-

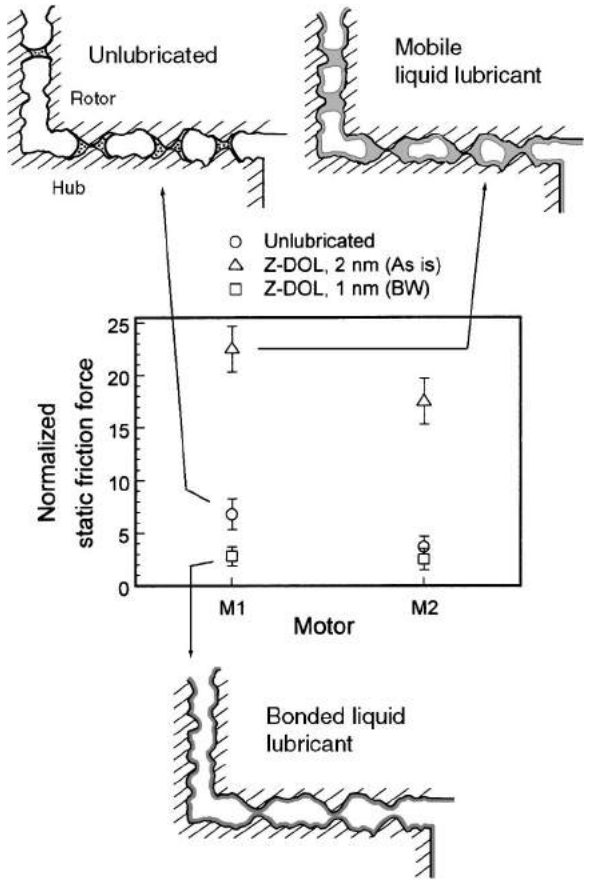

FIG. 46. Summary of effect of liquid and solid lubricants on static friction force of micromotors. Despite the hydrophobicity of the lubricant used (Z-DOL), a mobile liquid lubricant (Z-DOL as is) leads to a very high static friction force due to increased meniscus forces whereas a solid-like lubricant (bonded Z-DOL, BW) appears to provide some amount of reduction in static friction force (Ref. 89).

stiction tabs located at the center of a doubly clamped beam or at the end of a cantilever beam,[110] the use of side-wall spacers to reduce contact area,[111] by providing a hydrophobic surface,[112,113] and introducing roughness or bumps to the silicon substrate in order to reduce contact area.[114,115] Commonly used methods to overcome release stiction are dry release methods (e.g., CO_2 critical point drying or sublimation method). The work of adhesion per unit area for polysilicon beams released by the conventional evaporation method for drying has been reported to be 100 ± 300 $mJ\,m^{-2}$,[17] whereas the work of adhesion per unit area for polysilicon beams released by using supercritical CO_2 drying method is 1 ± 2 $mJ\,m^{-2}$.[21]

Another issue in the polysilicon surface micromachining is the formation of solid bridges. Chemical reactions at silicon surfaces immersed in water can lead to the formation of silica precipitates, which can form strong solid bridges during drying. Methods used to overcome adhesion due to this mechanism include formation of chemical oxide layer to protect silicon surfaces or coating the silicon surfaces with a thin ($\sim$200 nm) Si_3N_4 coating that can survive 10:1 HF release etch, thereby preventing the exposure of structural polysilicon.[80]

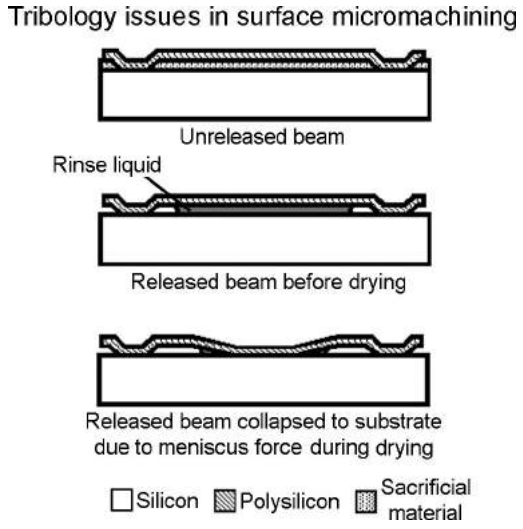

FIG. 47. Schematics of microstructures during fabrication using surface micromachining.

VI. SUMMARY

Adhesion between solids arises from the interatomic forces exerted across the interface. These forces may be strictly surface forces in the sense that they derive from the surface atoms themselves. Valence bonds provide surface forces. Surface charges also provide surface forces; these occur when ionic surfaces are in contact with other ionic solids. They will also occur if an electrically charged layer is formed at the interface, e.g., during sliding (the triboelectric effect). Metallic bonds can form primarily in metal±metal pairs. All solids will, in addition, experience adhesion due to van der Waals interactions between atoms below the surface layers. Hydrogen bonds can occur in polymers. Adhesion interactions may often be calculated in terms of free surface energies. The energy required to create new surface, expressed over an area consisting of many atoms in the surface lattice, is referred to as the free surface energy. The higher the surface energy of a solid surface, the stronger the bonds it will form with a mating material. One obvious suggestion is to select materials that have a low surface energy. The use of lubricants at the interface reduces the surface energy. Materials with low work of adhesion result in low adhesion, where work of adhesion represents the energy that must be applied to separate a unit area of the interface or to create new surfaces.

Broadly speaking, clean surfaces will adhere to most other clean surfaces. The real strength of hard solids is far lower than the theoretical strength because of the presence of surface ®lms, roughness, and lack of ductility leading to low real area of contact (as compared to apparent area of contact) as well as peeling apart of the contact due to elastic recovery during unloading. In general, highly elastic solids, such as polymers, adhere strongly if the surfaces are fairly smooth, in spite of the fact that the interfacial forces are relatively weak. Since the materials are soft and deformable they easily

give a large area of contact, and they can stretch appreciably under the in¯uence of released elastic stresses without rupturing.

Liquids that have a small contact angle or wet, such as water, will spontaneously condense from vapor as bulk liquid onto (hydrophilic) surfaces. The presence of the liquid ®lms of the capillary condensates or the pre-existing ®lm of the liquid can signi®cantly increase the adhesion between solids bodies. Liquid-mediated adhesive forces include meniscus force due to surface tension and a rate-dependent viscous force. A liquid between and around two contacting bodies results in the formation of curved (concave shaped) menisci (liquid bridges). The menisci should be concave for a liquid in between hydrophilic surfaces. The attractive meniscus force occurs because of the negative Laplace pressure inside the curved (concave) meniscus arises as a result of surface tension effects. The product of this pressure difference and the immersed surface area is the attractive meniscus force. The equilibrium meniscus force increases with an increase in the surface tension of the liquid. The viscous component of the liquid-mediated adhesive force increases with the liquid viscosity and decreases with the time to separate the two surfaces. Viscous force increases proportionally to the square root of the start-up velocity or cube root of the start-up acceleration for an interface that moves at constant velocity or constant acceleration (before separation), respectively. In the contact of two rough surfaces, meniscus force increases with an increase in relative humidity and/or liquid ®lm thickness and decrease of surface roughness of the interface. Selected non-Gaussian surfaces exhibit low meniscus forces.

In liquid-mediated contacts, high adhesion and static friction, and in some cases kinetic friction, is a function of meniscus and viscous contributions. Surface roughness, type of liquid and its ®lm thickness, rest time, and start-up acceleration affect the adhesion and static friction. Very high adhesion and static friction can be reached in very smooth surfaces in the presence of some liquid.

When two hydrophilic surfaces come in close proximity in the presence of a liquid ®lm, the intrinsic attractive force always consists of meniscus and van der Waals forces in addition to other sources. If the separation distance between the two surfaces is on the order of about 0.5 nm, van der Waals forces may be dominant compared to meniscus forces. van der Waals forces must be considered for separation distances up to about 2±5 nm. Meniscus forces operate up to the break of meniscus, ranging from 5 to 20 nm. van der Waals forces can be minimized by making surfaces rougher.

Adhesion measurements can be measured using a SFA or an AFM on micro- to nanoscales, respectively, between an AFM tip and the component and by using a microtriboapparatus between two components. A cantilever beam array technique can also be used to screen methods for adhesion reduction between two beams.

Adhesion and friction measurements on micro- and nanoscale on single-crystal silicon and three hydrophobic and low friction ®lms, DLC, chemically bonded Z-DOL, and HDT, show that these ®lms can reduce adhesion and friction of silicon. These ®lms can be used as anti-adhesion ®lms for MEMS/NEMS in different environments and operating conditions. The adhesion and friction data clearly show scale dependence. Several reasons for scale dependence are discussed.

A variety of techniques have been proposed and some are used in commercial applications to reduce stiction. If the source of high adhesion and static friction (stiction) is liquid mediated adhesion, then surface energy, the amount of mobile liquid present at the interface, and/or contact area need to be minimized. Surface energy can be reduced by providing a hydrophobic surface. The amount of mobile liquid can be reduced by using solid lubricants or partially chemically bonded liquid ®lms or by controlling relative humidity. The contact area can be reduced by introducing roughness or bumps on the surfaces and/or by having stiffer/harder surfaces, or by reducing the apparent size of one of the bodies. Stiction reduction is especially important in devices with smooth surfaces which involve relative motion under light loads. In these devices, in the presence of liquid ®lm, meniscus forces may be large and in some cases much larger than external load. In close proximity (0.5±5 nm), van der Waals forces may also be signi®cant. Examples of devices in which stiction is important include magnetic storage devices and MEMS/NEMS which involve relative motion.

ACKNOWLEDGMENT

The author would like to thank Dr. Huiwen Liu for a thorough reading of the manuscript.

[1]B. Bhushan, B. S. Sharma, and R. L. Bradshaw, ASLE Trans. **27**, 33 (1984).
[2]B. Bhushan, *Tribology and Mechanics of Magnetic Storage Devices*, 2nd ed. (Springer, New York, 1996).
[3]B. Bhushan, *Principles and Applications of Tribology* (Wiley, New York, 1999).
[4]B. Bhushan, *Introduction to Tribology* (Wiley, New York, 2002).
[5]A. W. Adamson, *Physical Chemistry of Surfaces*, 5th ed. (Wiley, New York, 1990).
[6]J. N. Israelachvili, *Intermolecular and Surface Forces*, 2nd ed. (Academic, San Diego, 1992).
[7]K. Miyoshi, D. H. Buckley, T. Kusaka, C. Maeda, and B. Bhushan, in *Tribology and Mechanics of Magnetic Storage Systems*, edited by B. Bhushan and N. S. Eiss (ASLE, Park Ridge, IL, 1988), pp. 12±16, SP-25.
[8]B. Bhushan and M. T. Dugger, ASME J. Tribol. **112**, 217 (1990).
[9]J. J. Bikerman, *The Science of Adhesive Joints* (Academic, New York, 1961).
[10]S. S. Voyutski, *Autoadhesion and Adhesion of High Polymers* (Wiley, New York, 1963).
[11]R. Houwink and G. Salomon, *Adhesion and Adhesives*, 2nd ed. (Elsevier, Amsterdam, 1967).
[12]*Physical Chemistry of Adhesion*, edited by D. H. Kaelble (Wiley Interscience, New York, 1971), pp. 22±83.
[13]B. V. Derjaguin, N. A. Krotova, and V. P. Smilga, *Adhesion of Solids* (translated from Russian by R. K. Johnston) (Consultants Bureau, New York, 1978).
[14]D. H. Buckley, *Surface Effects in Adhesion, Friction, Wear and Lubrication* (Elsevier, Amsterdam, 1981).
[15]D. Maugis, in *Principles of Tribology*, Modern Tribology Handbook, Vol. 1, edited by B. Bhushan (CRC Press, Boca Raton, FL, 2001), pp. 163± 203.
[16]N. Tas, T. Sonnenberg, H. Jansen, R. Legtenberg, and M. Elwenspoek, J. Micromech. Microeng. **6**, 385 (1996).
[17]R. Maboudian and R. T. Howe, J. Vac. Sci. Technol. B **15**, 1 (1997).

[18]B. Bhushan, *Tribology Issues and Opportunities in MEMS* (Kluwer Academic, Dordrecht, 1998).
[19]B. Bhushan, *Springer Handbook of Nanotechnology* (Springer, Heidelberg, 2004).
[20]M. P. de Boer and T. M. Mayer, MRS Bull. **26**, 302 (2001).
[21]K. Komvopoulos, J. Adhes. Sci. Technol. **17**, 477 (2003).
[22]W. M. van Spengen, Microelectron. Reliab. **43**, 1049 (2003).
[23]H. Liu and B. Bhushan, *Ultramicroscopy* (in press).
[24]F. J. Martin and C. Grove, Biomed. Microdevices **3**, 97 (2001).
[25]J. Woodley, Clin. Pharmacokinet **40**, 77 (2001).
[26]E. R. Beach, G. W. Tormoen, J. Drelich, and R. Han, J. Colloid Interface Sci. **247**, 84 (2001).
[27]W. A. Zisman, Ind. Eng. Chem. **55**, 19 (1963).
[28]J. Mahanty and B. W. Ninham, *Dispersion Forces* (Academic, New York, 1976).
[29]Anonymous, Mater. Sci. Eng. **83**, 169 (1986).
[30]M. Sikorski, Trans. ASME D **85**, 279 (1963).
[31]L. F. Cof®n, Lubr. Eng. 50 (1956).
[32]F. P. Bowden and G. W. Rowe, Proc. R. Soc. London, Ser. A **233**, 429 (1956).
[33]K. I. Johnson and D. V. Keller, J. Appl. Phys. **38**, 1896 (1967).
[34]J. S. McFarlane and D. Tabor, Proc. R. Soc. London, Ser. A **202**, 224 (1950).
[35]A. C. Moore and D. Tabor, Br. J. Appl. Phys. **3**, 299 (1952).
[36]W. D. Callister, *Materials Science and EngineeringÐAn Introduction* , 5th ed. (Wiley, New York, 1999).
[37]M. Hein and S. Arena, *Foundations of College Chemistry*, 10th ed. (Wiley, New York, 2003).
[38]A. Johnsen and K. Rahbek, J. Inst. Electr. Eng. **61**, 713 (1923).
[39]S. M. Skinner, R. L. Savage, and J. E. Rutzler, J. Appl. Phys. **24**, 438 (1953).
[40]D. K. Davies, J. Phys. D **6**, 1017 (1973).
[41]A. Wahlin and G. Backstrom, J. Appl. Phys. **45**, 2058 (1974).
[42]E. Rabinowicz, *Friction and Wear of Materials*, 2nd ed. (Wiley, New York, 1995).
[43]D. V. Keller, Wear **6**, 353 (1963).
[44]D. V. Keller, J. Adhes. **4**, 83 (1972).
[45]P. Richmond and B. W. Ninham, J. Low Temp. Phys. **5**, 177 (1971).
[46]B. V. Derjaguin, N. V. Chugrev, and J. M. Muller, *Surface Forces* (Consultants Bureau, New York, 1987).
[47]A. A. Meradudin and P. Mazur, Phys. Rev. **22**, 1684 (1980).
[48]R. S. Bradley, Philos. Mag. **13**, 853 (1932).
[49]A. I. Bailey, J. Appl. Phys. **32**, 1407 (1961).
[50]K. L. Johnson, K. Kendall, and A. D. Roberts, Proc. R. Soc. London, Ser. A **324**, 301 (1971).
[51]B. V. Derjaguin, V. M. Muller, and Y. P. Toporov, J. Colloid Interface Sci. **53**, 314 (1975).
[52]V. M. Muller, V. S. Yushchenko, and B. V. Derjaguin, J. Colloid Interface Sci. **77**, 91 (1980).
[53]V. M. Muller, B. V. Derjaguin, and Y. P. Toporov, Colloids Surf., A **7**, 251 (1983).
[54]D. Tabor, J. Colloid Interface Sci. **58**, 1 (1977).
[55]D. Maugis, J. Colloid Interface Sci. **150**, 243 (1992).
[56]K. N. G. Fuller and D. Tabor, Proc. R. Soc. London, Ser. A **345**, 327 (1975).
[57]K. Miyoshi and D. H. Buckley, in *Tribology and Mechanics of Magnetic Storage Systems*, edited by B. Bhushan and N. S. Eiss (ASLE, Park Ridge, IL, 1984), pp. 13±20, SP. 16.
[58]D. H. Buckley, in *Surface Films and Metallurgy Related to Lubrication and Wear*, Progress in Surface Science Vol. 12, edited by S. G. Davidson (Pergamon, New York, 1982), pp. 1±153.
[59]B. L. Weick and B. Bhushan, Tribol. Trans. **43**, 33 (2000).
[60]L. H. Lee, in *Effect of Surface Energetics on Polymer Friction and Wear*, Advances in Polymer Friction and Wear Vol. 5A (Plenum, New York, 1974), pp. 31±68.
[61]T. Stifter, O. Marti, and B. Bhushan, Phys. Rev. B **62**, 13667 (2000).
[62]S. T. Patton and B. Bhushan, IEEE Trans. Magn. **33**, 2513 (1997).
[63]C. Gao, X. Tian, and B. Bhushan, Tribol. Trans. **38**, 201 (1995).
[64]M. J. Matthewson, Philos. Mag. A **57**, 207 (1988).
[65]E. M. Williams (private communications).
[66]S. K. Chilamakuri and B. Bhushan, J. Appl. Phys. **86**, 4649 (1999).
[67]M. J. Matthewson and H. J. Mamin, Proc. Mater. Res. Soc. Symp. **119**, 87 (1988).
[68]C. A. Kotwal and B. Bhushan, Tribol. Trans. **39**, 890 (1996).
[69]X. Tian and B. Bhushan, J. Phys. D **29**, 163 (1996).
[70]S. K. Chilamakuri and B. Bhushan, Proc. Inst. Mech. Eng., Part J: J. Eng. Tribol. **212**, 19 (1998).
[71]B. Bhushan, U.S. Patent No. 5,737,229 (1998).
[72]B. Bhushan, U.S. Patent No. 6, 007 896 (1999).
[73]B. Bhushan, *Handbook of Micro/Nanotribology*, 2nd ed. (CRC Press, Boca Raton, FL, 1999).
[74]B. Bhushan and C. Dandavate, J. Appl. Phys. **87**, 1201 (2000).
[75]H. Liu and B. Bhushan, J. Vac. Sci. Technol. A **21**, 1528 (2003).
[76]C. H. Mastrangelo and C. H. Hsu, *Proceedings of the Solid State Sensor and Actuator Workshop* (IEEE, New York, 1992), pp. 208±212.
[77]C. H. Mastrangelo and C. H. Hsu, J. Microelectromech. Syst. **2**, 44 (1993).
[78]C. H. Mastrangelo, in *Tribology Issues and Opportunities in MEMS*, edited by B. Bhushan (Kluwer Academic, Dordrecht, 1998), pp. 367±395.
[79]M. P. de Boer and T. A. Michalske, J. Appl. Phys. **86**, 817 (1999).
[80]R. L. Alley, G. J. Cuan, R. T. Howe, and K. Komvopoulos, in Ref. 76, pp. 202±207.
[81]B. Bhushan, A. V. Kulkarni, V. N. Koinkar, M. Boehm, L. Odoni, C. Martelet, and M. Belin, Langmuir **11**, 3189 (1995).
[82]B. Bhushan and Z. Zhao, J. Inf. Storage Process. Syst. **1**, 1 (1999).
[83]B. Bhushan, Diamond Relat. Mater. **8**, 1985 (1999).
[84]B. Bhushan, *Modern Tribology Handbook, Vol. One: Principles of Tribology, Vol. Two: Materials, Coatings and Surface Treatments* (CRC Press, Boca Raton, FL, 2001).
[85]B. Bhushan and H. Liu, Phys. Rev. B **63**, 245412 (2001).
[86]B. Bhushan, H. Liu, and S. M. Hsu, ASME J. Tribol. (in press).
[87]H. Liu and B. Bhushan, Ultramicroscopy **91**, 185 (2002).
[88]H. Liu and B. Bhushan, Ultramicroscopy **97**, 321 (2003).
[89]S. Sundararajan and B. Bhushan, J. Vac. Sci. Technol. A **19**, 1777 (2001).
[90]Z. Zhao and B. Bhushan, Wear **202**, 50 (1996).
[91]C. Gao and B. Bhushan, Wear **190**, 60 (1995).
[92]Z. Zhao and B. Bhushan, IEEE Trans. Magn. **34**, 1708 (1998).
[93]B. Bhushan and S. Sundararajan, Acta Mater. **46**, 3793 (1998).
[94]U. D. Schwarz, O. Zwoerner, P. Koester, and R. Wiesendanger, in *Micro/Nanotribology and its Applications*, edited by B. Bhushan (Kluwer Academic, Dordrecht, 1997), pp. 233±238.
[95]J. Ruan and B. Bhushan, ASME J. Tribol. **116**, 378 (1994).
[96]B. Bhushan, J. N. Israelachvili, and U. Landman, Nature (London) **374**, 607 (1995).
[97]B. Bhushan and M. Nosonovsky, Acta Mater. **51**, 4331 (2003).
[98]B. Bhushan, Adv. Inf. Storage Syst. **5**, 175 (1993).
[99]S. Chilamakuri and B. Bhushan, Wear **230**, 11 (1999).
[100]A. C. Tam and B. Bhushan, J. Appl. Phys. **61**, 1646 (1987).
[101]T. A. Core, W. K. Tsang, and S. J. Sherman, Solid State Technol. **36**, 39 (1993).
[102]R. E. Sulouff, in *Tribology Issues and Opportunities in MEMS*, edited by B. Bhushan (Kluwer Academic, Dordrecht, 1998), pp. 109±120.
[103]L. J. Hornbeck and W. E. Nelson, *Spatial Light Modulators and Applications*, OSA Technical Digest Series Vol. 8 (1988), pp. 107±110.
[104]L. J. Hornbeck, Proc. Soc. Photo-Opt. Eng. **3634**, 158 (1999).
[105]L. J. Hornbeck, MRS Bull. **26**, 325 (2001).
[106]R. A. Robbins and S. J. Jacobs, U.S. Patent No. 6,300,294 B1 (2001).
[107]M. Ferrari and J. Liu, Mech. Eng. Dec. 44 (2001).
[108]G. T. Mulhern, D. S. Soane, and R. T. Howe, *Proceedings of the International Conference on Solid-State Sensors and Actuators* (IEEE, New York, 1993), pp. 296±299.
[109]C. H. Mastrangelo and G. B. Saloka, *Proceedings IEEE Micro Electro Mechanical Systems* (IEEE, New York, 1993), pp. 77±81.
[110]T. Abe and M. L. Reed, J. Micromech. Microeng. **6**, 213 (1996).
[111]F. S. A. Sandejas, R. B. Apte, W. C. Banyai, and D. M. Bloom, *Proceedings of Seventh International Conference on Solid-State Sensors and Actuators* (IEEE, New York, 1993), pp. 6, 7.
[112]M. R. Houston, R. Maboudian, and R. T. Howe, *Proceedings of the Eighth International Conference on Solid-State Sensors and Actuators* (IEEE, New York, 1995), pp. 210±213.
[113]P. F. Man, B. P. Gogoi, and C. H. Mastrangelo, *Proceedings IEEE Micro Electro Mechanical Systems* (IEEE, New York, 1996), pp. 55±60.
[114]L. S. Fan, Y. Tai, and R. S. Muller, Sens. Actuators **20**, 41 (1989).
[115]C. H. Mastrangelo, Tribol. Lett. **3**, 233 (1997).
[116]C. Y. Poon and B. Bhushan, Wear **202**, 68 (1996).